Electric Field Calculations on Dry-Type Medium Voltage Current Transformers

by

Sandeep Kumar Lakshmichand Jain

A Thesis Presented in Partial Fulfillment
of the Requirements for the Degree
Master of Science

Approved June 2012 by the
Graduate Supervisory Committee:

Ravi Gorur, Chair
George Karady
Raja Ayyanar

ARIZONA STATE UNIVERSITY

August 2012

ABSTRACT

This research presents potential and electric field calculations on medium voltage (MV) epoxy insulated outdoor current transformers (CTs) using a numerical calculation approach. Two designs of MV dry-type epoxy insulated CTs were modeled using 3D field simulation software COULOMB® 9.0. Potential and electric fields were calculated based on boundary element method. Different conditions such as dry exterior surface, wet exterior surface and internal voids were considered. The research demonstrates that the presence of internal conductors in CTs results in a less severe surface electric field distribution when compared to outdoor insulators of the same voltage range and type. The high electric field near the exited end triple-point of the CT reduces. This remained true even under wet conditions establishing better outdoor performance of CTs than outdoor insulators which have no internal conductors. The effect of internal conductors on voids within the insulation structure was also established. As a down side, internal voids in CTs experience higher electric field stress than in conductor-less insulators. The work recognizes that internal conducting parts in dry type CTs improves their outdoor performance when compared to electrical equipment without internal conductors.

ACKNOWLEDGEMENTS

I would like to express my sincerest gratitude to my advisor, Dr. Ravi Gorur, whose encouragement, guidance and support has enabled me to write this thesis. I also want to express my gratitude to Dr. George Karady and Dr. Raja Ayyanar for their time and consideration in being a part of my graduate supervisory committee.

I would like to acknowledge ABB Inc. personnel Mr. Hoan Le and Mr. Pentti Mahonen for providing the samples, drawings and technical input towards the thesis.

I especially want to thank my parents Mr. Lakshmichand Jain and Mrs. Sunanda Jain, Mr. Jinendra Lakshmichand and Ms. Kavya Nandakumar for the continual inspiration and motivation to pursue my utmost goals.

Finally, I would like to thank my fellow power system students for their continuous advice and encouragement.

TABLE OF CONTENTS

Page

Page

LIST OF TABLES

Table Page

LIST OF FIGURES

Figure Page

Figure Page

NOMENCLATURE

MVCT	Medium Voltage Current Transformers
IT	Instrument Transformer
MV	Medium Voltage
CT	Current Transformer
SF6	Sulfur hexafluoride
I_p	current in the primary circuit (ampere)
N_p	number turns in the primary circuit (turns)
I_s	current in the secondary circuit (ampere)
N_s	number turns in the secondary circuit (turns)
PT	Potential Transformer
Z_b	impedance of the burden (ohms)
P_b	volt-ampere rating of the burden (volt-amperes)
I_{sb}	rated secondary short-circuit current (amperes)
PD	Partial Discharge
HV	High Voltage
E	electric field intensity (volts/meter)
D	electric flux density (coulombs/meter^2)
H	magnetic field intensity (amperes/meter)

B	magnetic flux density (webers/meter^2)
J	electric current density (amperes/meter^2)
ρ	electric charge density (coulombs/meter^3)
ϵ	permittivity (farads/meter)
μ	permeability (henrys/meter)
σ	conductivity (siemens/meter)
$\hat{u}$	unit vector normal to the interface pointing away from the conductor
ΔE	change in electric field intensity (volts/meter)
ΔD	change in electric flux density (coulombs/meter^2)
ΔH	change in magnetic field intensity (amperes/meter)
ΔB	change in magnetic flux density (webers/meter^2)
J_s	surface electric current density (amperes/meter^2)
ρ_s	surface electric charge density (coulombs/meter^3)
CSM	Charge Simulation Method
FEM	Finite Element Method
BEM	Boundary Element Method
n	Number of individual charges
Q_j	Magnitude and polarity of j^{th} charge
$\emptyset_i$	potential at any point i
P_{ij}	potential coefficients form point i to charge j
$\mu_{\_}$	unknown value which is applied to a shape function

K	co-efficient of μ_ obtained by weighted least squares method
$B_$	terms included in Poisson's equations and boundary conditions
F	weighted function at each node
$\frac{\partial F}{\partial n}$	normal derivative of the weighted function at each node
P	potential at each node
$\frac{\partial P}{\partial n}$	normal derivative of the potential at each node
$[H]$	known NxN full asymmetric matrix of $\int_{\Gamma} \frac{\partial F}{\partial n} d\Gamma$
$[G]$	known NxN full asymmetric matrix of $\int_{\Gamma} F \, d\Gamma$
U	potential vector
Q	normal derivative vector of the potentials
Hz	Hertz
LV	Low Voltage
(x_i, y_i, z_i)	global coordinates of an element in the study domain
(x_{il}, y_{il}, z_{il})	coordinates of l^{th} geometric node within an element
(ξ, η)	local coordinates of an element in the elemental domain
$\beta_l(\xi, \eta)$	Lagrangian biasing functions
m	number of geometric nodes in an element
ϵ_c	complex permittivity
ω	angular frequency (radians/second)

Chapter 1. INTRODUCTION

1.1. Introduction to medium voltage current transformers

Medium Voltage Current Transformers (MVCTs) fall under the broad category of transformers known as Instrument Transformers (ITs). MVCTs are utilized to transform current from the high values in the distribution systems to low values that can be measured using low-voltage measuring instruments. The voltage range considered as MV is from 34.5 kV to 10 kV primary and 5 amperes or less is usually measured in the short circuited secondary [1].

MVCTs are used for three main functions: to feed distribution system protective equipment and relays, to provide input signal to control systems that manage the distribution system and to operate monitoring devices for quality checks and billing purposes. They are reliable devices with no moving parts that have an average life span of over 25 years [1]. Based on their insulating material, they are of two basic types: Liquid-immersed – oil dielectric medium, Dry-type – gas or solid dielectric medium.

The dry-type transformer market is expected to increase due to the several advantages of dry-type units over liquid-immersed units. Few of those advantages are listed below [2].

i. Insulation systems used in dry-type transformers enable operation at higher temperatures than those used in liquid-immersed units which are prone to catch fire.

ii. Being dry they can be positioned in any orientation as opposed to a vertical orientation of liquid-immersed transformers.

iii. Dry-type solid insulation units provide manufactures higher flexibility to mold the insulation system in different shapes and leakage distances.

iv. Lower capital investments required to build dry-type transformers encourage investors as there is higher return on investment.

SF6 is the most widely used gaseous insulating material for dry-type CTs. They have favorable dielectric properties, but pose an environmental hazard. As distribution systems are usually around populated areas, the potential of SF6 gas leaking and causing a health hazard is higher. Synthesized polymer resigns like epoxy are often preferred as insulating medium for dry-type CTs. Polymer materials are light weight, malleable, have high resistance to pollution and pose a lesser environmental risk. They have been used for over 30 years for outdoor insulation purposes [3]. The disadvantage of using polymer for insulation is that they degrade with time. Any imperfections inside or moisture on the surface grow over time and the overall life of the CT reduces. Due to the presence of internal conductors in CTs, polymer insulation in CT is expected to perform differently when compared to polymer insulation systems in electrical equipment with no internal conductors. This difference is researched and presented as part of this thesis.

1.2. Research objectives

This work aims to demonstrate the competency of numerical calculation techniques to model and study insulation systems in electrical equipment with complex geometries. Numerical techniques are especially useful when laboratory experiments are time consuming and have high costs. The aim is not to replace experiments, for they are an essential tool for all electrical analysis, but to reduce the time and number of experiments required to arrive at conclusive results. Specific objectives of this research are listed below.

i. Calculating and comprehensively studying the electric field and potential distribution on dry-type MV current transformers.
ii. Simulating different real life scenarios like dry conditions, wet conditions and presence of internal voids on dry-type MV current transformers.
iii. Determining if different conductor geometries making the insulation in CTs exhibit different electric behavior. Two CT geometries are modeled for this purpose.
iv. Investigating the effect of internal conductors present in CTs on the surface potential and electric field distribution.
v. Determining the effect of internal conductors on electric field stresses observed inside voids in the insulation system.

1.3. Scope and content

This thesis documents the models, results and conclusions from the study of electric field and potential distribution on dry-type MV polymer insulated CTs. For the purpose of this thesis, CTs with primary voltage of 15 *kV* line to line are modeled. This study is limited to the conditions experienced by CTs used in protective and metering applications at the distribution level. Results are specified for current transformers and may not be applicable to potential transformers of the same *kV* range or type.

Chapter 2 describes the characteristics of CTs, their basic working principle, various components, and possible cause of insulation failure.

Chapter 3 describes the various techniques to obtain knowledge of electric field. Electrical measurement, analytical calculation and numerical calculation techniques are described.

Chapter 4 gives the details of the two dry-type MV current transformers modeled, conditions studied and modeling and result validation approach.

Chapter 5 presents comparative graphs plotting the potential and electric field distribution for the various conditions described in Chapter 4. A discussion on the results and how they compare is also reported.

Chapter 6 summarizes the results obtained and concludes the thesis. A direction for future research is also proposed.

Chapter 2. REVIEW ON CURRENT TRANSFORMERS

2.1. Introduction

Current Transformers (CTs) are inherently identical to conventional two-winding transformers in that they possess a pair of electrically isolated but magnetically coupled windings disposed around a magnetic core. They differ from conventional transformers in terms of their application. CTs are low power devices utilized for scaling down high currents to enable their measurement. Their core construction differs for this reason from conventional two-winding transformers. This chapter describes the working principle, components and causes of insulation failure of CTs.

2.2. Working principle

In the CT, alternating current applied to the low-turns primary winding attempts to magnetize the central core but by doing so, an electro motive force and current is induced on the high-turns secondary winding which opposes the magnetization of the core. This phenomenon where the secondary current opposes the magneto motive force which produces it is known as Lenz's law [4].

Ampere-turns is a quantity which is obtained by multiplying the current in a coil with the number of turns in the coil. If losses are neglected, the ampere-turns of the primary circuit in a CT is exactly equal to the ampere-turns of the secondary circuit. Hence, by knowing the number of primary and secondary turns and measuring the current in the secondary winding, the current flowing in the

primary winding can be determined. This relationship, neglecting losses, can be written as,

$$I_p \times N_p = I_s \times N_s$$

$$I_p = \frac{I_s \times N_s}{N_p}$$

where,

I_p = current in the primary circuit (ampere)

N_p = number turns in the primary circuit (turns)

I_s = current in the secondary circuit (ampere)

N_s = number of turns in the secondary circuit (turns)

The usual number of turns in the primary circuit (N_p) is 1 or 2. And the number of turns in the secondary circuit (N_s) is decided such that the maximum current measured in the secondary (I_s) does not exceed 5 amperes. In all CTs, $N_s \gg N_p$ to obtain a sufficiently low current in the secondary circuit. This is the basic principle behind the working of CTs.

2.3. Components

The essential components of any CT are,

i. Primary winding connected in series with the circuit, the current of which is to be determined

ii. Secondary winding which has current induced on it proportional to the current in the primary winding

iii. Magnetic core to couple the primary and the secondary winding

iv. Burden, short circuit secondary impedance

v. Insulation system that envelops the primary, secondary and core

2.3.1. Primary winding

In typical CTs, the primary winding is of two types: single-turn winding and multi-turn winding. Low turns are kept so as to obtain a sufficiently low current induced in the high-turns secondary winding, the relationship of which has been described earlier. Since the current carried by the primary winding is high, thick conductors are used. This is an observable difference between CTs and potential transformers (PTs). The single-turn primary winding has many advantages when compared to multi-turn winding. The principal one being that, single-turn winding experiences less thermal and dynamic stress when compared to a multi-turn winding. Multi-turn winding are used only in situations where performance of a required value is desired [5].

2.3.2. Secondary winding

The secondary winding of a CT comprises of large number of uniformly distributed coils wound around a magnetic core. Current induced in the secondary winding is proportional to and much lower than that flowing through the primary winding. Since the impedance of the secondary winding is part of the secondary circuit's impedance, and sometime is of the same order as that secondary impedance [5], it is an important factor in determine the CT's performance.

2.3.3. Magnetic core

The core plays the important role of magnetically coupling the primary and the secondary winding. In ideal CTs 100% coupling is assumed, however some percentage of coupling is lost due to leakage of flux. This loss is determined by the material used to construct the core. Typically, iron is used as core material.

Another important factor in the designing of the core is the frequency of excitation [5]. The frequency affects the time it takes for the core to saturate and should be considered while designing the core.

2.3.4. Burden

Any instrument or electrical equipment connected to the secondary of the CT is called the burden of the CT. It has an impedance related to it and is not termed as load because its function is different from that of a load. CTs are never operated in open circuited secondary. Unless a burden is attached to it, CT secondary is shot circuited to avoid very high voltages to develop in the secondary circuit. Burdens are specified in volt-amperes units at rated shot-circuit current. The ohmic impedance of the burden is computed using the following relation [5],

$$Z_b = \frac{P_b}{{I_{sb}}^2}$$

where,

Z_b = impedance of the burden (ohms)

P_b = volt-ampere rating of the burden (volt-amperes)

I_{sb}= rated secondary short-circuit current (amperes)

Knowing the power factor of the burden in use, the burden resistance and reactance can be computed.

Manufacturers of CTs need to know the burden value so as to check its performance. Higher burdens usually result in better CT performance [5]. However an unrealistically high value may cause CT core saturation, a situation that is to be avoided. Therefore, care is taken to specify an apt burden value.

2.3.5. Insulation system

Insulation system is the backbone of any electrical equipment. The insulation system of the CT holds the primary windings, central core and the secondary winding in place and facilitates its safe installation and use. The insulation system is the focus of the research reported in this thesis. Though it directly does not affect the measuring accuracy of the CT, the insulation system highly influences its life and reliability. Figure 1 shows the common insulation systems used for the construction of CTs [6].

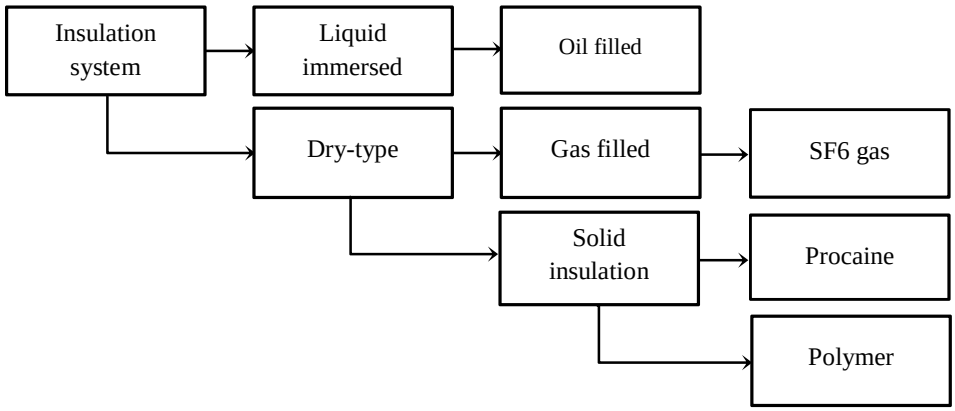

Figure 1. Common types of insulation systems

As discussed in chapter 1, dry-type insulation systems are favored for use in MV applications at distribution levels. The dry-type insulation systems are of two types: gas filled insulation and solid insulation systems. While gas filled insulation requires SF6 gas (a potentially hazardous chemical), solid insulation systems are manufactured using porcelain or polymer. As porcelain has a higher mass density than polymer [6], their use results in heavier units whose installation and transportation costs are higher. High performance polymer insulators have been used for over 3 decades [3] due to their low weigh and high resistance to pollution, factors that are drawbacks while using porcelain. With the anticipated increase in use of synthesized polymer resins in mind, this research attempts to study the influence of internal conductors (primary winding, core and secondary winding) on surface wetting and structural voids in epoxy insulated CTs.

2.4. Insulation system failure

The insulation system failure problems encountered in CTs are not very different than those encountered on other insulated electrical equipment. The only difference would be the presence of isolated charged conductors in the CT resulting in different stresses experienced on the insulation system. As mentioned earlier, organic insulating materials like epoxy are extensively used in the construction of dry-type CTs, which is the insulation system researched and presented in this thesis. Due to the organic nature of insulation, dry-type CTs are prone to degradation over time. The degradation process hastens in the presence of moisture and manufacturing defects. The aspect of contamination and moisture affecting

the outdoor performance of non-ceramic insulators has been extensively studied [7], [8]. Insulation problems encountered on dry-type CTs are, in general, no different from those encountered in other dry-type insulated electrical equipment. Being low power devices, overheating is not the major reason for insulation failure. Instead, dry -band arcs are partial discharges have higher probability of causing insulation breakdown in CTs. The following sections describe these two phenomena.

2.4.1. Dry-band arcing

Pollution, ultraviolet radiation, acid rain and surface discharges are common causes of insulators degradation when subjected to outdoor conditions. Of these causes, surface discharges have a high impact on insulator degradation [9]. Discharges initiate when moisture on the surface of an insulator starts to change shape under electrical stress [10]. When the wetting rate of the insulator surfaces is less than the drying rate, dry bands form at locations where current densities are high [11]. If sufficient voltage drops exist in these dry bands, permanent arcs may form. These arcs may propagate to a complete insulation flashover or quench due to insufficient current flow. Reference [12] describes the life cycle of dry band formation, arc initiation and subsequent conditions required for flashover, on a post type insulator.

Under persistent surface discharge, the insulating material degrades and tends to lose its hydrophobicity [13]. This loss of hydrophobicity leads to immi-

nent dry-band arcing. Extensive levels of dry-band arcing are also detrimental to insulator condition and amount of current flow, potentially leading to failure and flashover [14]. Voltage and current are important factors in the initiation and persistence of the arc. Due to the presence of isolated internal conducting parts in CTs, the phenomena of dry-band arcing is expected to be different when compared to outdoor insulators or bushings. For MVCTs studied in this research, the effect of surface wetting on electric field and potential distribution is examined.

2.4.2. Partial discharge

The phenomenon of Partial Discharge (PD) is one that reduces the mechanical strength of insulations systems in all types of electrical equipment. Otherwise referred to as corona discharge, PD occurs when imperfections exist within or on the surface of insulation systems. Due to the presence of imperfections, localized electric field stress increases which cause ionization of the medium and subsequent electron discharges results. As the name suggests, PD doesn't cause sudden or short term insulation failure. If the discharges persist over long periods of time, slowly but surely insulation failure occurs.

PD has been extensively studied for outdoor insulators and mitigating approaches can be found in the literature [15]. The addition of a conductor rings on outdoor bushings has helped reduce localized electric field stress, as reported in [16]. One of the most common cases of insulation breakdown is the presence of air voids or crevices within the structure. According to Paschen's law a break-

down voltage of about 300 V is required in air under atmospheric pressure to create a spark [17]. For MV systems, like one studied in this research, this 300 V can be generated across voids in the insulation system, therefore resulting in partial discharge activity.

Manufactures of insulated electrical equipment go through great lengths to avoid internal air voids or crevices while building the insulation systems. Causing gradual insulation deterioration, PD activity in voids is usually undetected during insulation testing phases and appears over time as the voids get bigger due to the presence of arcs within them. For MVCTs considered for this research, PD activity due to internal voids in the presence of embedded conductors is studied.

Chapter 3. ELECTRIC FIELD CALCULATION TECHNIQUES

3.1. Introduction

Electric field distribution inside and on the surface of insulation system is not constant, but vary non-linearly with distance from the electrode. Due to the phenomenon of dielectric refraction between materials of different dielectric constants, the electric flux lines leaving an electrode (having high dielectric constant □ = infinity) into an insulating material (having a lower dielectric constant), leaves the electrode perpendicular to its surface [17]. This causes high electric field stress at the electrode-insulator boundary and results in a non-linear distribution of electric field. It is also observed that the electric field increases with increase in the number of intersecting material boundaries [17]. In most insulated systems, there are only three boundaries (insulator-conductor-air) usually referred to as triple-point, which exhibit high electric field stress [17].

Primary objective of the analysis and design of all insulation systems is to make sure that the maximum electric field stress is equal to or lower than the breakdown strength of all the insulating materials (including air) [17]. A compromise in this objective would result in insulation failure thereby causing heavy damage to, or inaccurate working of insulated electric equipment. It can be realized that the knowledge of electric field distribution is key in designing and studying insulation systems.

Several methods can be used to obtain the values of electric field stresses. They are categorized into: experimental methods, analytical methods and numerical methods, each having their own advantages and disadvantages. While experimental techniques use approximate real physical models or the actual system itself to measure definite quantities, analytic or numerical methods use the best-fit theoretical models that most accurately represent the actual phenomenon studied. The following sections describe the methods in more detail.

3.2. Experimental methods

Accurately designed laboratory experiments have been used extensively to measure electric field stress. Due to the availability of actual real-time data measurement, experimental techniques are the most trusted and thus widely used methods for validation of theoretical or computer simulated results. Electrolytic tank experiment and impedance networks experiment are examples of experimental for electric field measurement [17]. Experiments are also useful when analytical models are inaccurate or when computation availability is limited for iterative numerical calculations.

Though experimental methods are key in validating results, they are most often not chosen as the first option in finding the electric field stress. This can be due to lack for resources, time constrains or absence of good experimental designs. Analytic methods and numerical methods are now widely used to calculate electric field stress. While in experimental methods actual quantities are meas-

ured, in analytical or numerical methods electrical field stress is calculated based on theorized formulas and electromagnetic laws.

3.3. Analytical methods

Analytical calculation techniques give exact results by solving mathematical formulas that represent simple physical phenomena. Mathematical formulas have been derived for calculation of electric field stress around co-axial cables and conductors [19] which have simple geometries. Design calculations of many insulation apparatus were, for a long time, done using analytically derived formulas. However, developing accurate formulas for electric field calculation on equipment with complex geometries is tedious and would require a lot of resources. As the need for more sophisticated design tools increased, iterative numerical methods were developed to model complex geometries and non-homogeneous regions [20] which analytically derived formulas are incapable of.

3.4. Numerical methods

Electric field stress is described by equations which are complex and difficult to solve analytically. A bypass is to solve for a solution using an iterative numerical approach. A few decades ago, this computationally demanding approach would have been considered impractical. However, with improvements in computer technology in the last few decades, the use of numerical methods is no longer unrealistic and often preferred for the calculation of electric field.

Maxwell's partial differential equations are used to model all electromagnetic field calculation problems. The equations are solved subject to a set of equations that represent boundary conditions. The boundary conditions imposed make the solution inhomogeneous. By using Green's function, suitable changes are made on the boundary conditions and Maxwell's equations such that in the solution is homogeneous. These steps form the basis of all field simulation methods [20].

Maxwell's equations

Maxwell's equations are a set of fundamental equations that govern all electromagnetic phenomena. The equations can be represented in both integral and differential forms, but this thesis only refers to the integral form. Maxwell's equations in integral form are given by [20],

$$\oint_C E \,.\partial l = -\frac{\partial}{\partial t}\iint_S B.\partial s \qquad \text{(Faraday's law)}$$

$$\oint_C H\,.\partial l = -\frac{\partial}{\partial t}\iint_S D.\partial s + \iint_S J.\partial s \qquad \text{(Maxwell-Ampere law)}$$

$$\oiint_S D\,.\partial s = \iiint_V \rho\partial v \qquad \text{(Gauss's law)}$$

$$\oiint_S B\,.\partial s = 0 \qquad \text{(Gauss's law - magnetic)}$$

where,

E = electric field intensity (volts/meter)

D = electric flux density (coulombs/meter2)

H = magnetic field intensity (amperes/meter)

B = magnetic flux density (webers/meter2)

J = electric current density (amperes/meter2)

ρ = electric charge density (coulombs/meter3)

When conducting material is present, another governing equation called the equation of continuity is added [20].

$$\oiint_S J \,.\, \partial s = -\frac{\partial}{\partial t} \iiint_V \rho \partial v \qquad \text{(equation of continuity)}$$

Maxwell's equations form an underdetermined problem, where the number of unknowns is more than the number of equations. For the problem to be well defined, three more equations determining the relationship between field quantities are added.

$D = \epsilon E$ where ϵ = permittivity (farads/meter)

$B = \mu H$ where μ = permeability (henrys/meter)

$J = \sigma E$ where σ = conductivity (siemens/meter)

Boundary conditions

Complete representation of any electromagnetic field computation problem must include a set of boundary conditions along with the Maxwell's equations. A solution is arrived by solving the Maxwell's equations subject to the boundary conditions of the domain under consideration. For this thesis, two boundary conditions are considered [20],

At the interface between two surfaces: At each dielectric boundary, the potential and the normal component of the flux density must be same when viewed from either side of the boundary.

$$\hat{u} \,.\, \Delta E = 0$$

$$\hat{u} \,.\, \Delta D = \rho_s$$

$$\hat{u} \,.\, \Delta H = J_s$$

$$\hat{u} \,.\, \Delta B = 0$$

where,

$\hat{u}$ = unit vector normal to the interface

ΔE = change in electric field intensity (volts/meter)

ΔD = change in electric flux density (coulombs/meter2)

ΔH = change in magnetic field intensity (amperes/meter)

ΔB = change in magnetic flux density (webers/meter2)

J_s = surface electric current density (amperes/meter2)

ρ_s = surface electric charge density (coulombs/meter3)

At a perfectly conducting surface: At each electrode boundary, the potential must be equal to the known conductor potential. If one of the medium making an interface is a perfect conductor, the boundary conditions are now [20],

$$\hat{u} \times E = 0$$

$$\hat{u} \,.\, B = 0$$

where,

$\hat{u}$ = unit vector normal to the interface pointing away from the conductor

E = exterior electric field intensity (volts/meter)

B = exterior magnetic flux density (webers/meter2)

This boundary condition establishes that a perfect conductor carries charge only on its surface and cannot sustain internal fields. The equations change for an imperfect conductors but this thesis assumes perfect conductors.

Greens function

The electromagnetic field computation problem is inhomogeneous both because of the Maxwell's partial differential equations that describe it and also because of the boundary conditions it is subjected to. Green's function is a type of function used to solve inhomogeneous differential equations subject to specific initial conditions [20]. The application of Green's function on partial differential equations can be understood as an analogy to the application of Fourier series on ordinary differential equations. The basic role of the Green's function is to make suitable changes on the partial differential equations and boundary conditions so as to attain a solution which is homogeneous.

The use of Maxwell's equations, boundary condition and Green's function is the basis of all field simulation methods. Famous among those are, Charge Simulations Method (CSM), Finite Element Method (FEM) and Boundary Element Method (BEM). All have their own advantages and disadvantages and the choice of simulation method used varies depending on the complexity of the prob-

lem and available resources. The following sections give more details on each method.

3.4.1. Charge Simulation Method (CSM)

Basic Principle

The basic principle of charge simulation method is that, if the magnitude and position of several discrete charges is known, potential and electric field at any other position (other than where the charges are places) can be calculated [21]. The type of discrete charges vary from point, line to ring charges, changing based on the type of geometry under consideration. If Q_j are n number of individual charges (point, line or ring) and $\emptyset_i$ is potential at any point i in the same space, then according to the superposition principle,

$$\emptyset_i = \sum_{j=1}^{n} P_{ij} Q_j \qquad \text{(superposition principle)}$$

where,

$P_{ij} =$ potential coefficients form i to j

Potential coefficients can be calculated analytically by knowing the position of the charges for different charge type (point, line, ring, etc.). Thus, defining the type and locations of the charges, a relationship between $\emptyset_i$ and Q_j can be determined at any boundary point. When this procedure is applied to m points with n number of discrete charges, the following system of equations form,

$$\begin{bmatrix} P_{11} & P_{12} & \cdots & P_{1n} \\ P_{21} & P_{22} & & P_{2n} \\ \vdots & & \ddots & \vdots \\ P_{m1} & P_{m2} & \cdots & P_{mn} \end{bmatrix} \begin{bmatrix} Q_1 \\ Q_2 \\ \vdots \\ Q_n \end{bmatrix} = \begin{bmatrix} \emptyset_1 \\ \emptyset_2 \\ \vdots \\ \emptyset_m \end{bmatrix}$$

$m \times n \qquad n \times 1 \quad m \times 1$

If the number of points where potential and electric field need to be calculated (contour points) m equals the number of simulating charges n, a critically determined linear problem is molded using the above matrix formulation. By already knowing the position of the discrete charges, and calculating the magnitude of the various charges $Q_{1..n}$, potential and therefore electric field can be computed at all the m contour points. It is however, necessary to confirm that the charges calculated comply with the boundary conditions and that the contour points do not lie on the same positions as those occupied by the discrete charges.

Advantages

By choosing a large number of contour points (larger than the number of discrete charges), this method can provide a very accurate solution. For simple problems, an error of less than 0.01% can be achieved in calculating the potentials [22]. This method has been used to calculate electric fields for three phase systems as reported in [23], [24].

Disadvantages

Problem formulation is complicated and requires a lot of time and experience. The choice of individual charge type, number of charges and position highly

influence the accuracy and time to arrive at a solution. The solution is highly sensitive to small changes in input [22].

3.4.2. Finite Element Method (FEM)

Basic principle

The finite element method is a technique for computing approximate solutions to boundary-value problems. The solution domain is considered to be an accumulation of finite number of discrete intervals interconnected at nodal points [20].

As detailed earlier, electromagnetic phenomena is expressed using a set of governing equations (Maxwell's equations) and boundary conditions. These equations are approximated and a set of simultaneous equations are formed. These simultaneous algebraic equations are difficult to form for a large domain. Piecing the domain into smaller elements, forming and solving the algebraic equations for each element individually, is the basic idea behind the finite element method. Finally, by connecting elements together, the unknown quantity (electric potential in this case) is calculated by interpolating over the entire structure in a piecewise fashion [20]. Electric fields can then be calculated with ease.

The choice of element shape can vary from simple two dimensional triangles to three dimensional cubes. If a linear triangular element is considered having

3 nodes; i, j and k, then, with a help of weighted function principle, the elemental linear equation can be formulated in a matrix from as below,

$$\begin{bmatrix} K_{ii} & K_{ij} & K_{ik} \\ K_{ji} & K_{jj} & K_{jk} \\ K_{ki} & K_{kj} & K_{kk} \end{bmatrix} \begin{bmatrix} \mu\_i \\ \mu\_j \\ \mu\_k \end{bmatrix} = \begin{bmatrix} B\_i \\ B\_j \\ B\_k \end{bmatrix}$$

where,

$\mu\_$ = unknown value which is applied to a shape function to give the potential

K = co-efficient of μ obtained by weighted least squares method

$B\_$ = source terms included in Poisson's equations and the boundary conditions

Finally, by assembling the element matrix equations for all the elements, a giant system matrix is formed in which the K matrix is sparse and symmetric positive definite. By decomposition of the giant K matrix and evaluating the values of $\mu\_$ at all nodal interconnections, potential at each node is calculated.

Advantages

The method is very flexible and can be applied to the complex geometries. It is capable of giving highly accurate results depending on the number of elements considered. Since the matrix to be inverted is sparse and symmetric positive definite, a lot of memory space and computation time is saved.

Unlike other numerical methods like charge simulation method which simulates charges, this method directly computes potential. This method has many applications in designing electric insulation equipment like insulators and bushing, as reported in [25].

Disadvantages

Finite element method is an iterative approach to a solution thus requiring a convergence criterion and an error check. It divides the entire domain including the boundaries and volumes formed by the boundaries. For domains with large boundaries, number of elements considered becomes extremely large resulting in an increase in computational burden [20].

3.4.3. Boundary Element Method (BEM)

Basic principle

From the governing Maxwell's equations, integral equations are derived on the boundary surfaces. These boundary integral equations, which are mathematically equivalent to the original partial differential equations, are solved based on the principle of weighted residuals, where the fundamental solution is chosen as the weighted function [26]. The unknowns, the values of the weighted function and its normal derivatives along the boundaries, are solved simultaneously using a matrix formulation.

Considering 2-dimentional triangular elements to discretize the boundary surfaces, if Γ represents the surface of a triangular element and F represents fundamental solution of the governing equation along the surface, then equation formed for the chosen triangular element would be [20],

$$\int_{\Gamma} \frac{\partial F}{\partial n} d\Gamma \times P = \int_{\Gamma} F \, d\Gamma \times \frac{\partial P}{\partial n} \text{ or}$$

$$H \times u = G \times q$$

where,

F = weighted function at each node (known quantity)

$\frac{\partial F}{\partial n}$ = normal derivative of the weighted function at each node (known quantity)

P = potential at each node (unknown quantity)

$\frac{\partial P}{\partial n}$ = normal derivative of the potential at each node (unknown quantity)

For N number of elements, a matrix equivalent is formed to solve for the unknown potential vector (U) and normal derivative vector of the potentials (Q). The matrix equation is as shown below [20],

$$[\ H\ ]\ U = [\ G\ ]\ Q$$

where,

[H] = known NxN full asymmetric matrix of $\int_{\Gamma} \frac{\partial F}{\partial n} d\Gamma$

[G] = known NxN full asymmetric matrix of $\int_{\Gamma} F\, d\Gamma$

P = unknown potential vector of size N

Q = unknown normal derivative vector of the potentials of size N

The most important feature of the boundary element method (which sets it apart from the finite element method) is that, it eliminates the need for dividing the entire domain volume and only the domain boundary surfaces are discretized into smaller manageable elements [26]. Therefore, only surface integrals are solved and not volume integrals. Due to its unique advantages, this is the method chosen for the research done in this thesis.

Advantages

Unlike the finite element method, a very accurate solution is achieved as no interpolation of data is required using this method. As only surfaces are discretized and integrated, the dimension of the problem reduces by one [26]. This makes it a very useful tool for open boundary problems. Many electric field computation problems, which are mostly unbounded, are solved using this method, as reported in [27], [28].

Disadvantages

This method may require more memory as the matrix formed is asymmetric and full. Singularity of the matrix may also occur and needs to be dealt with [26].

Chapter 4. MODELING APPROACH AND CASE DESCRIBTION

4.1. Model description

Two different types of CTs are modeled in an attempt to avoid model dependency on the results obtained. The primary porous of any CT design is to ensure that adequate magnetic coupling occurs between the primary and the secondary winding without saturation of the core. The type and dimensions on the central core plays an important role in the accuracy and performance of CTs [29]. This section details the model dimensions and material properties of the two CTs studied for this research.

4.1.1. Model-A: Toroid core and single-turn primary

Primary and secondary windings are positioned around a toroid shape core, insulated using epoxy and assembled on an aluminum support frame. This type of core design is employed to minimize secondary leakage reactance and thus assist in keeping the losses to a minimum. It avoids air gaps in the magnetic circuit as secondary windings of one or more layers are wound with uniform distribution. Salient features of this model are tabulated in Table 1.

Table 1. Salient features of Model-A CT

Normal System Voltage	15 kV line-line
Basic Impulse Level Voltage	110 kV
Application	Outdoor
Rated Primary Current	200 amperes
Rated Secondary Current	5 amperes
Frequency	60 Hz

Figure 2 shows Model A's internal conductor and external insulation material properties.

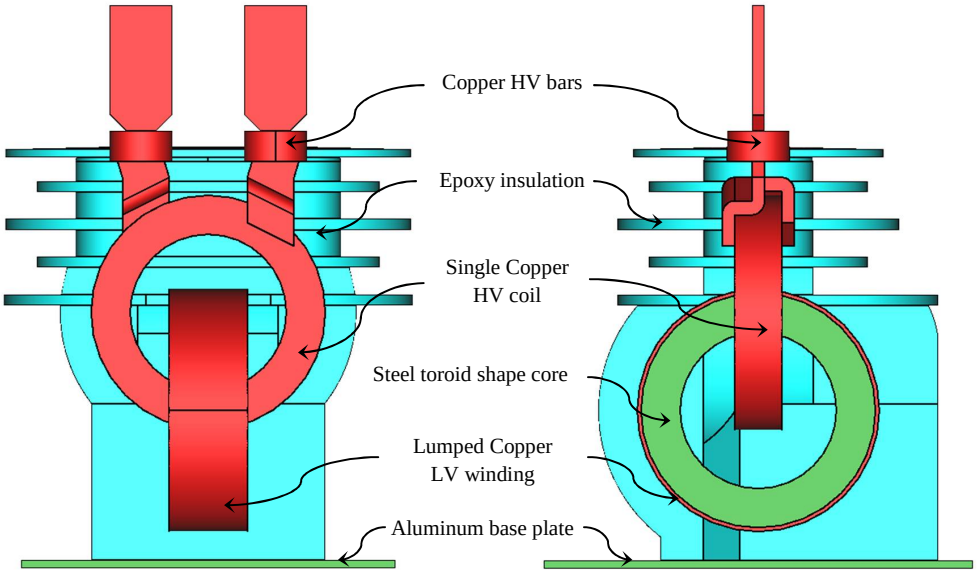

Figure 2. Model-A material properties

The bars supporting the central core are neglected for ease of modeling. The secondary winding is represented as a lump around the toroid shaped core. Table 2 summarizes the materials and their connections.

Table 2. Model-A material properties and connections

	Electrically conductive	**Relative permittivity**	**Connection**
Copper HV terminal bars	Yes	-	High voltage
Epoxy insulation	No	4.0	-
Copper HV coil	Yes	-	Grounded
Copper LV winding	Yes	-	Grounded
Steel core	Yes	-	Grounded
Aluminum base plate	Yes	-	Grounded

The major dimensions used for Model-A is given in Figure 3. All units are in millimeters.

Dry arc length	265 *mm*
Max. leakage distance	633 *mm*
Min. leakage distance	720 *mm*

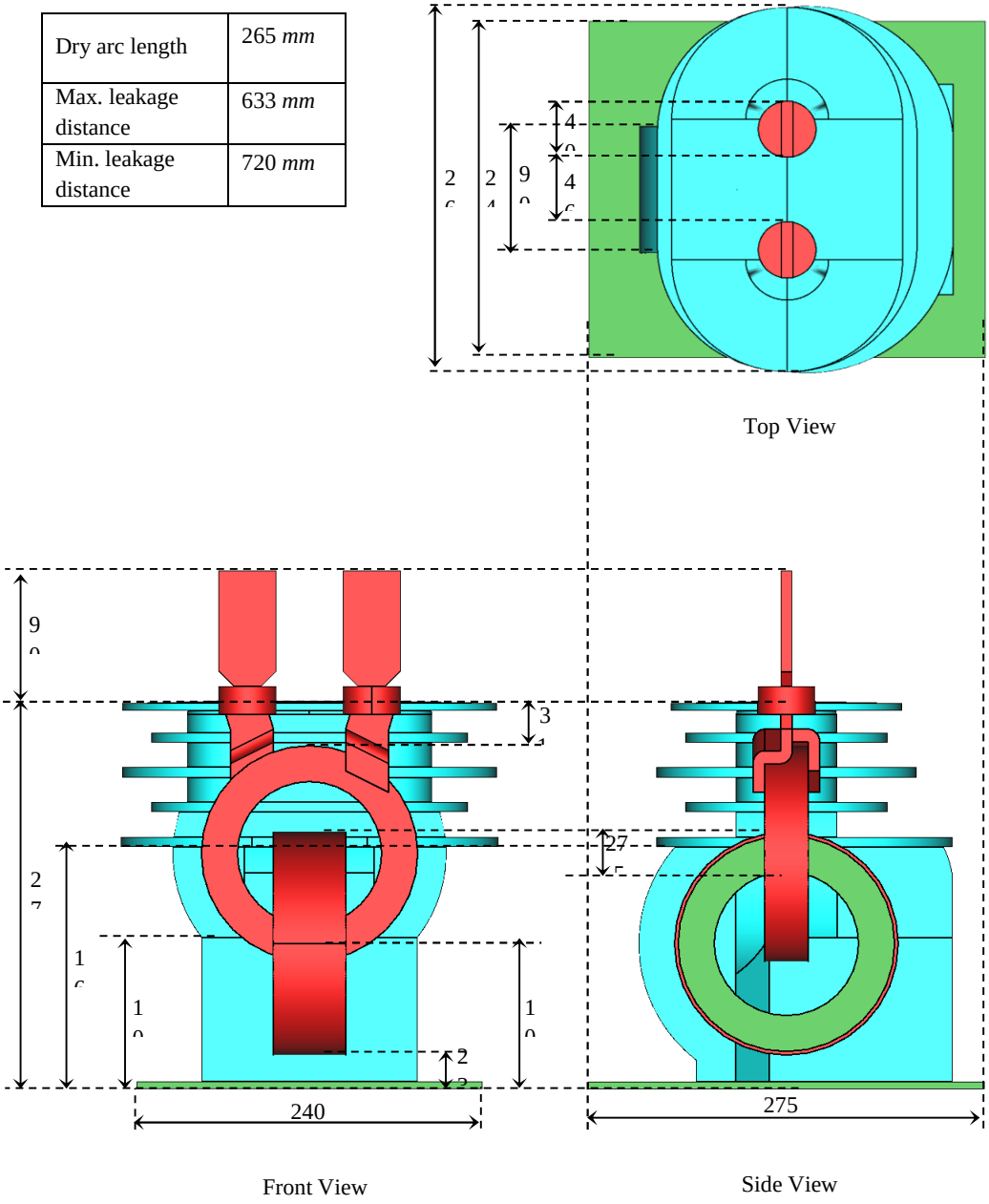

Figure 3. Major dimensions of Model-A CT

4.1.2. Model-B: Rectangle core and dual-turn primary

Core made up of rectangular strips are employed to build relatively less expensive CTs at the expense of performance. Primary terminals are located at the top of a high voltage bushing to provide sufficient creepage length. The secondary winding is centrally located within the primary winding and both are positioned on a rectangle shape core. The entire assemble is enveloped by epoxy insulation material and supported on an aluminum plate. Salient features of this model are tabulated in Table 3.

Table 3. Salient features of Model-B CT

Normal System Voltage	15 kV
Basic Impulse Level Voltage	110 kV
Application	Outdoor
Maximum Primary Current	600 amperes
Maximum Secondary Current	5 amperes
Frequency	60 Hz

Figure 4 shows Model B's internal conductor and external insulation material properties.

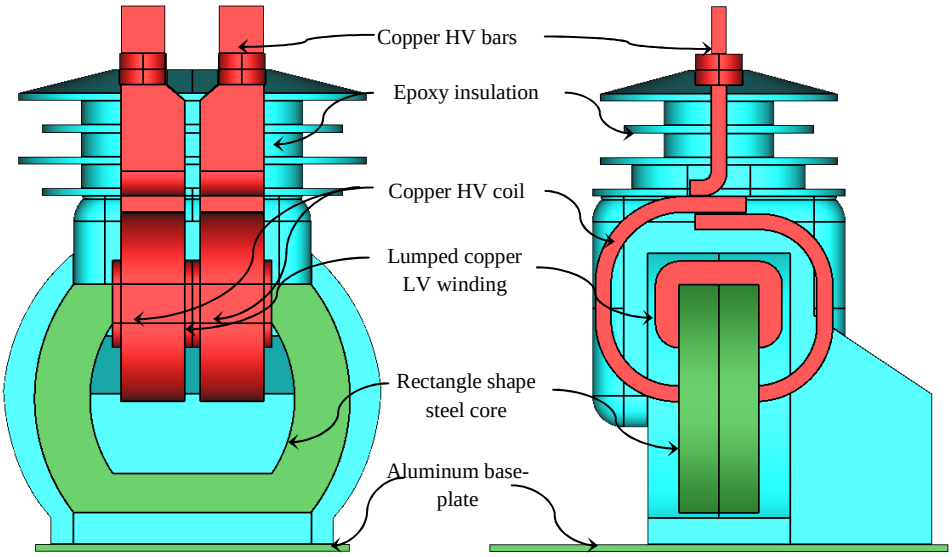

Figure 4. Model-B material properties

The bars supporting the central core are neglected for ease of modeling. The secondary winding is represented as a lump around the rectangular shaped core. Table 4 summarizes the materials and their connections.

Table 4. Model-B material properties and connections

	Electrically conductive	**Relative Permittivity**	**Connection**
Copper HV terminal bars	Yes	-	High voltage
Epoxy insulation	No	4.0	-
Copper HV coil	Yes	-	Grounded
Copper LV winding	Yes	-	Grounded
Steel core	Yes	-	Grounded
Aluminum baseplate	Yes	-	Grounded

The major dimensions used for Model-B is given in Figure 5. All units are in millimeters.

Dry arc length	300 *mm*
Max. leakage distance	592 *mm*
Min. leakage distance	550 *mm*

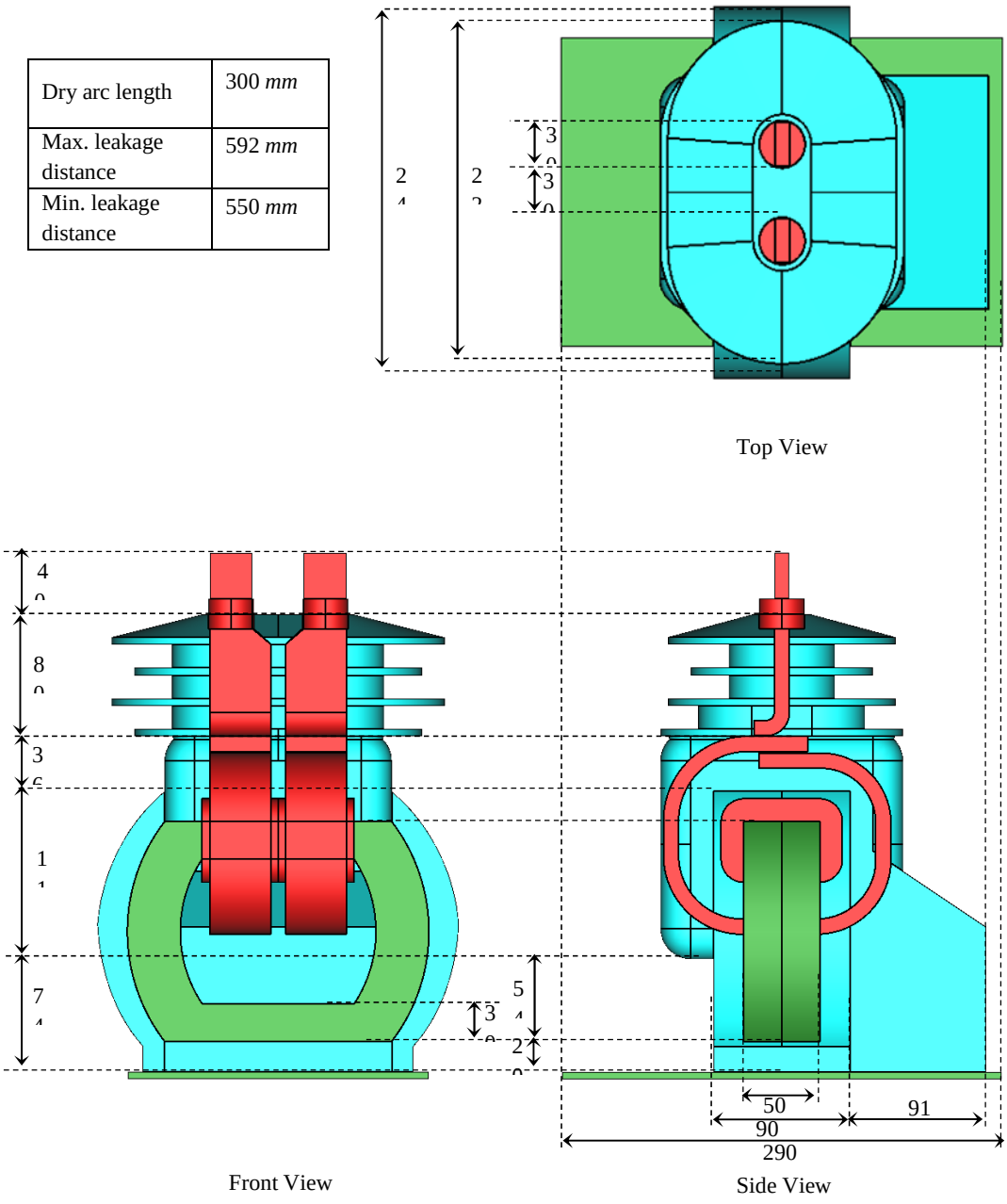

Figure 5. Major dimensions of Model-B CT

4.2. Case description

A total of 24 simulations are modeled as part of this thesis to model conditions like dry surface, wet surface and presence of internal voids in the insulation system. The cases are detailed in this section.

4.2.1. Study area

After running a few preliminary simulations, the leakage distances shown in Figure 6 are chosen as the study area for all calculations on the surface of both the CT. For Model-A CT, its maximum leakage distance is chosen and for Model-B its minimum leakage distance is chosen.

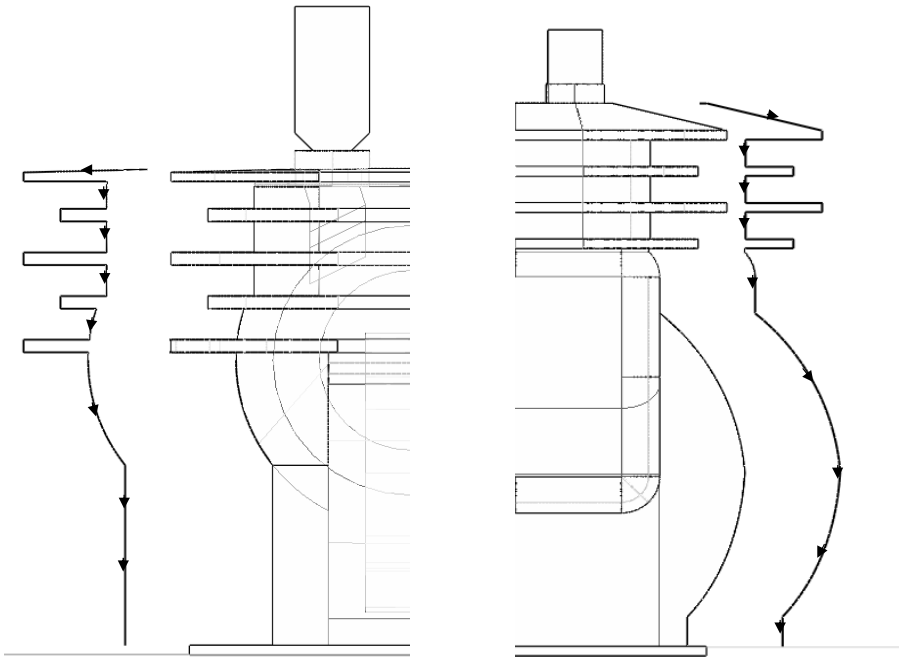

Figure 6. Leakage distances studied

4.2.2. Case 1: Dry surface

To reproduce electric behavior on CTs having a clean dry surface, simulations are run on both Model-A and Model-B CTs to calculate electric field and potential on their respective leakage distances. The case attempts to analyze the effect of internal conductors on CT performance under dry conditions. For this reason, simulations are re-run with internal conductors removed and replace by overlying epoxy insulation. Electric field and potential along respective leakage distances are recalculated.

Summarizing Case 1, a total of 2 simulations are modeled for Model-A and Model-B each and electric field and potential is calculated.

i. Dry surface and embedded internal conductors
ii. Dry surface and internal conductors removed

4.2.3. Case 2: Wet surface

Moisture on the surface of the insulation system results in high localized electric field stress and subsequent arcing occurs if electric field stress is close to 1.5 *kV/mm* [30]. For this case, simulations are run by including a wet film of moisture on the surface around the study area for each CT models. Similar to Case 1, simulations are re-run with internal conductors replaced by insulation material to analyze their absence on surface electric field under wet outdoor conditions.

Depending on the property of the insulating material and on the wetting rate, wetting on the surface can be partial or continuous. Both these situations are simulated as part of Case 2 by introducing a broken or partial film of moisture and a continuous film of moisture along studied areas of each CT model. Figure 7 shows the same.

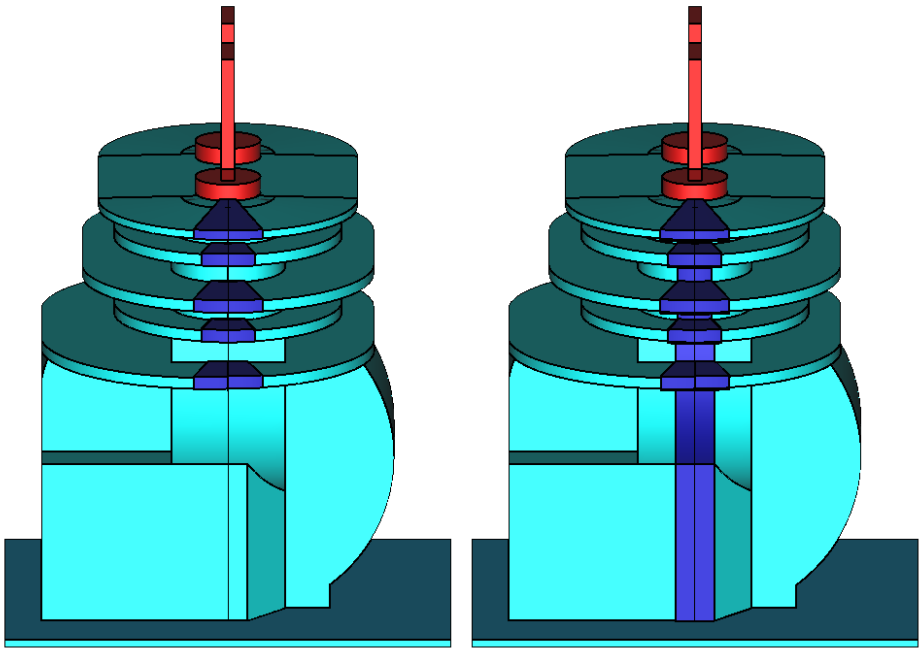

Partial Water Film Continuous Water Film

Figure 7. Partial and continuous water film on Model-A

The conductivity of moisture is not the same at all areas where the studied CTs may be installed. Near coastal areas, moisture with higher conductivity is present than further inland due to the presence of sault. To incorporate this possibility, the conductivity of the wet films (for both partial and continuous film) is changed between 1 $\mu S/cm$ to 200 $\mu S/cm$ and all calculations are made again.

Summarizing Case 2, a total of 8 simulations are run for Model-A and Model-B each and electric field and potential is calculated.

i. Partial wetting with 1 $\mu S/cm$ conductivity and embedded internal conductors
ii. Partial wetting with 200 $\mu S/cm$ conductivity and embedded internal conductors
iii. Partial wetting with 1 $\mu S/cm$ conductivity and internal conductors removed
iv. Partial wetting with 200 $\mu S/cm$ conductivity and internal conductors removed
v. Continuous wetting with 1 $\mu S/cm$ conductivity and embedded internal conductors
vi. Continuous wetting with 200 $\mu S/cm$ conductivity and embedded internal conductors
vii. Continuous wetting with 1 $\mu S/cm$ conductivity and internal conductors removed
viii. Continuous wetting with 200 μS/cm conductivity and internal conductors removed

4.2.4. Case 3: Internal voids

Partial discharge in voids in the insulations system of dry type CTs cause imminent dielectric breakdown and failure of the insulating material. As part of

this case, a set of 2 air voids placed at different locations in the insulation system as shown in Figure 8 and electric filed calculations are made 20 mm from the surface of the insulation system. The simulation is re-run with internal conductors removed to analyses the effect of internal conductors on structural voids.

Summarizing Case 3, 1 simulation is run on each dry CT model having voids spread at different sections of the insulation structure.

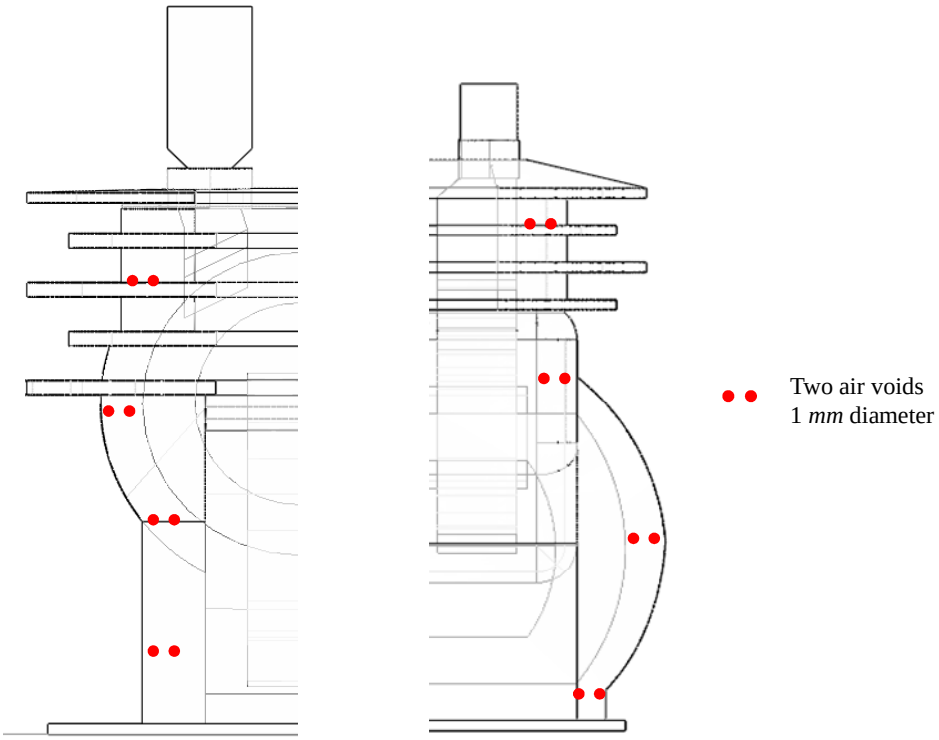

Figure 8. Air voids in Model-A and Mode-B insulation system

4.3. Modeling approach

The work reported in this thesis utilizes a software package named COULOMB 9.0 based on BEM, which is based on boundary integral equations and the

principle of weighted residuals. To solve the electric field integral equation, the surface *S* is discretized into a mesh of elements connected by nodes. Considering 2 dimensional triangular elements, each element is converted from its global co-ordinates (*x, y, z*) to its local coordinates (ξ, η) for ease of interpolation and numerical integration [31]. The triangular elements are mapped into different sizes based on the aspect ratios of different surfaces forming the volume in the study domain. The mapping is done using Lagrangian shape function as shown [31],

$$x_i = \sum_{i=1}^{m} \beta_l(\xi,\eta) x_{il}$$

$$y_i = \sum_{i=1}^{m} \beta_l(\xi,\eta) y_{il}$$

$$z_i = \sum_{i=1}^{m} \beta_l(\xi,\eta) z_{il}$$

where,

(x_i, y_i, z_i) = global coordinates of an element in the study domain

(x_{il}, y_{il}, z_{il}) = coordinates of l^{th} geometric node within an element

(ξ, η) = local coordinates of an element in the elemental domain

$\beta_l(\xi, \eta)$ = Lagrangian biasing functions

m = number of geometric nodes in an element (3 for triangles)

Equations are formed for all elements and solved simultaneously using a matrix formulation. The matrix thus formed is asymmetric and full with possible singularity conditions. COULOMB 9.0 handles singularities by further dividing them and using transformation techniques to remove them [31].

4.3.1. Modeling material properties

Material properties are introduced as known values in the solution by incorporating the following material characteristics which can be found in any materials handbook,

i. relative permittivity (ϵ_r)

ii. conductivity (σ)

Both these properties for any material is incorporated into a solution by using the complex form of permittivity [32], which is,

$$\epsilon_c = \epsilon'_r + i\left(\frac{\sigma}{\omega}\right)$$

where,

ϵ_c = complex permittivity

ϵ'_r= real part of complex permittivity (farads/meter)

σ = conductivity of the material (siemens/meter)

ω = angular frequency (radians/second)

4.3.2. Modeling surface wetting

Moisture on surfaces is modeled by incorporating a thin film of volume with thickness 1 mm and relative permittivity of 80. For the purpose of this thesis, wet films are modeled as volumes on the surface of the insulation system along its leakage distance and incorporated as part of the study domain. Figure 9 shows how moisture is modeled along the leakage distance of a CT and how 2D triangles are spread around to form a complete electrostatic field problem.

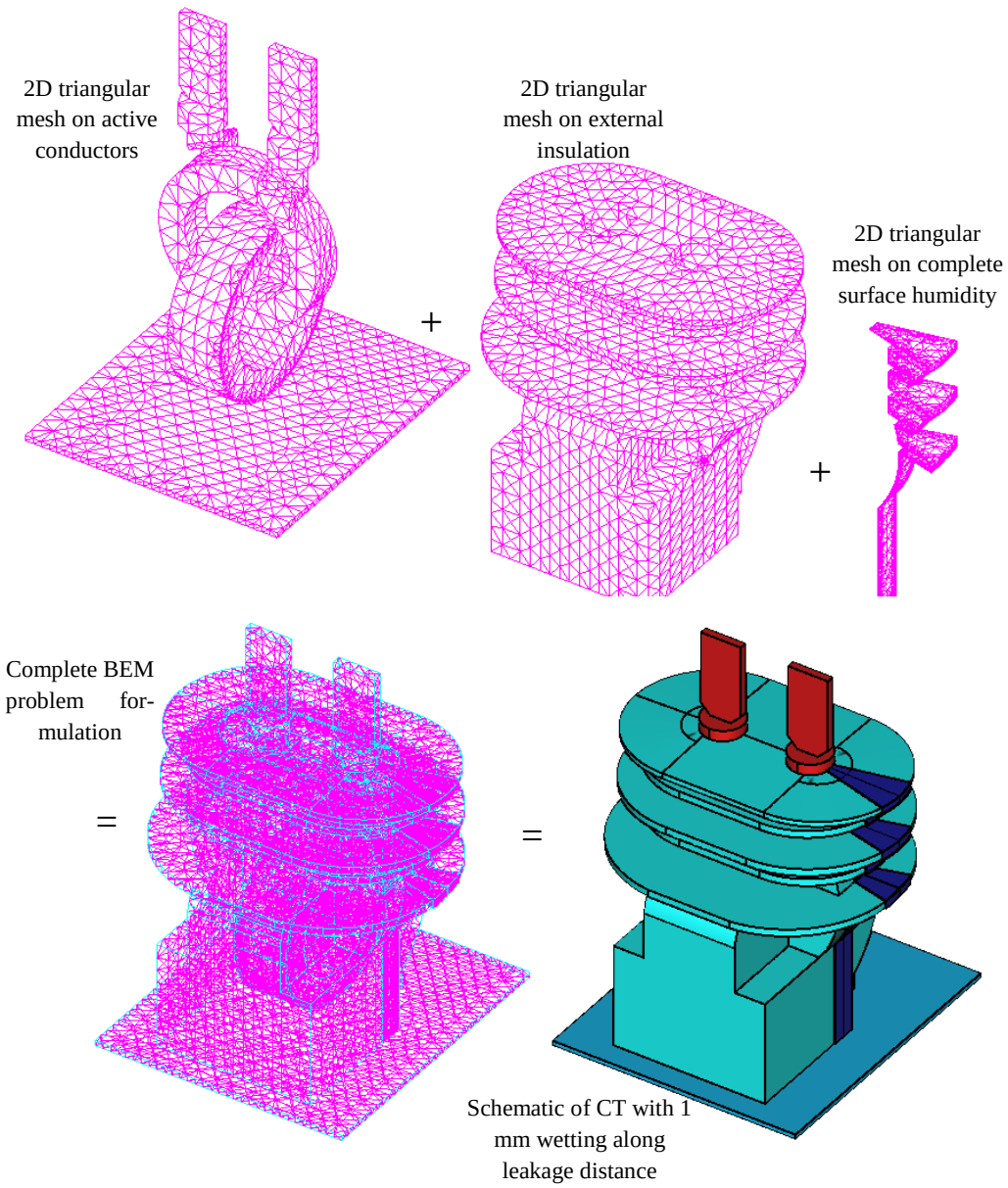

Figure 9. BEM problem formulation including surface wetting

The relative permittivity of water used is 80 and conductivity is varied from 1 to 200 micro siemens/centimeter to simulate cases described in the earlier sections.

4.3.3. Modeling internal voids

Spherical air voids are modeled along the chosen sections on each CT as described in Case 3. The diameter of the voids used is 1 millimeter with relative permittivity of 1.

4.4. Error validation

Since simulations are run to calculate electric field based on BEM, the limitations of the method causes errors in the solution obtained. It is important to validate the results based on practical engineering institution and mathematical and physical checks. The following list shows validation procedure followed for validating the results.

i. With regard to potential calculations, engineering judgment suggests that as calculations are made along the leakage distances of CTs, the value obtained further away from charged conductors would be lesser than those calculated closer to conductors.

ii. As electric fields calculated along the leakage distance are derivatives of the potential calculations, the vector integral of the electric field should give back the applied voltage. The electric field distribution plots along the leakage distances of CTs are integrated to verify if the applied voltage is obtained. An error of 3% or less is tolerated.

iii. For the research reported in this thesis, BEM with 2D triangular elements are used. Varying the number of triangles influences the accu-

racy of the solution. Different number of triangular elements is used to validate if the same solution is obtained. An error of less than 3% is tolerated.

iv. The tangential component of the electric fields calculated along the leakage distance of CTs must be equal both inside and outside the insulation system (boundary condition). An error of less than 3% is tolerated.

v. The normal component of the electric fields calculated along material boundaries must be proportional to the inverse of the ratios of known dielectric constants. An error of less than 3% is tolerated.

Chapter 5. RESULTS AND DISCUSSION

5.1. Introduction

All simulations were solved for varying number of 2D triangular element and the results obtained validated the various error checks for about 30000 2D triangular elements distributed around the entire study domain.

System configured with Intel Core 2 Due 64 bit processor working on Windows 7 OS with 4 GB of RAM was used for running all the simulations. The average time take for a single run was about 3 hours. The results for each case are reported in this chapter.

5.2. Case 1: Dry surface

This section shows the voltage and electric field distribution calculations made on dry Model-A and Model-B along their respective leakage distances. Figure 10 and Figure 11 show the potential and electric field distribution on Model-A and Model-B CT respectively. The primary voltage applied was the line to ground voltage of 8.66 *kV*. The calculations were made from the HV end to Ground plate mapping the entire leakage distance.

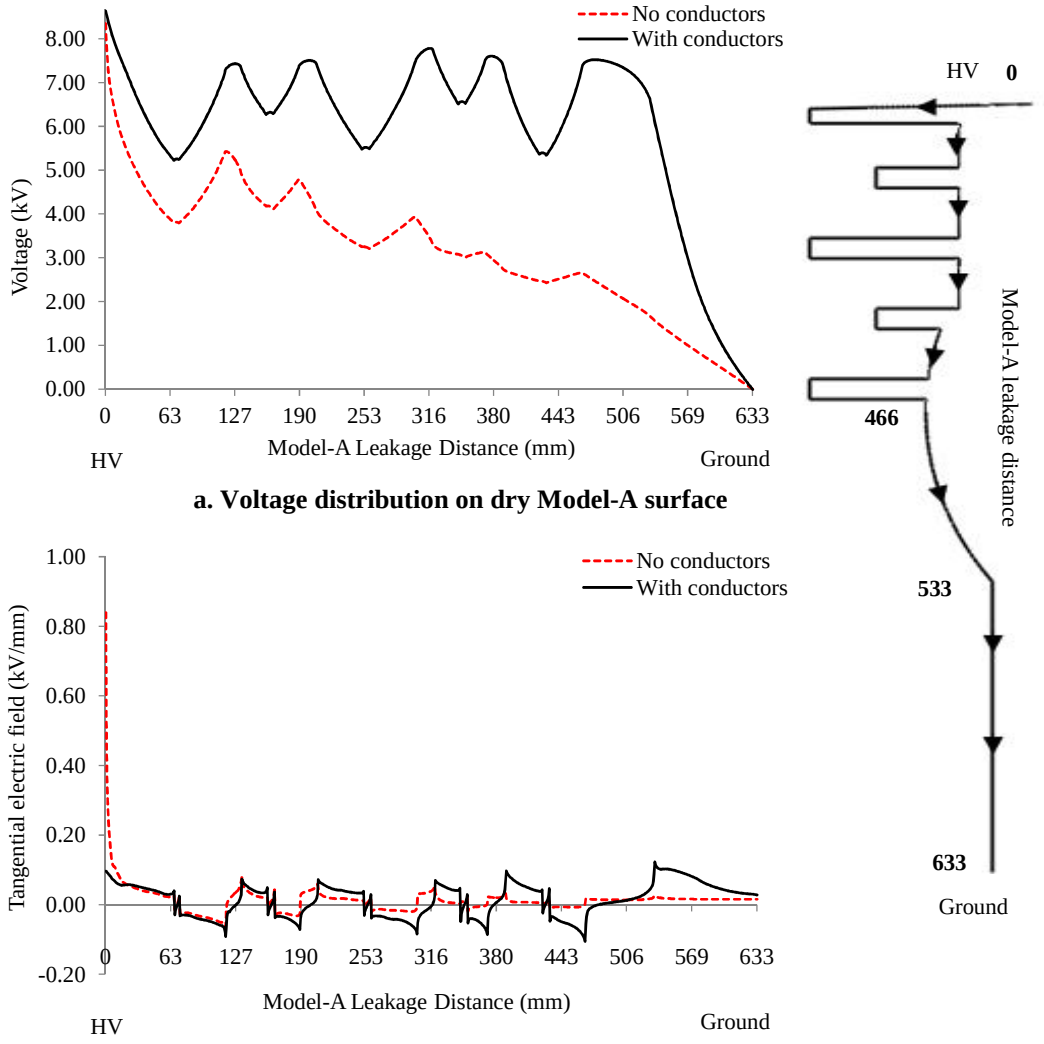

a. Voltage distribution on dry Model-A surface

b. Electric field distribution on dry Model-A surface

Figure 10. Voltage and electric field distribution on dry Model-A

From the voltage distribution plot in Figure 10, high surface potential close to ground is observed for the case with conductors. This is due to the potential of the primary winding which extends into the insulation system. It can also be observed that as potential calculations are made along the leakage distance, the voltage dips while moving away and rises again when calculations are made

closer to the primary terminal, thus causing a set of V-shaped curves representing potential along the five sheds of Model-A. Further inspection of the voltage plot reveals that, as the second and fourth shed have a shorter extension outward, the second and fourth V-shape is smaller than the rest. This is only observed for the case with internal conductors as the primary terminal and windings in Model-A extend into its insulation system. With regard to the potential plot with no conductors, the V-shape is only predominant along the first shed as the internal charged primary conductors are removed.

From the electric field distribution plot in Figure 10, it is observed that, for the case with conductors, electric field is distributed along the entire leakage length such that no specific point experiences high electric field stress. The maximum stress experienced is less than 0.2 *kV/mm*. Electric field calculated for the case with no internal conductors, however, is not evenly distributed as there is relative high field stress near the HV end. The electric field stress is close to 0.8 *kV/mm* at HV end for the case with no internal conductors.

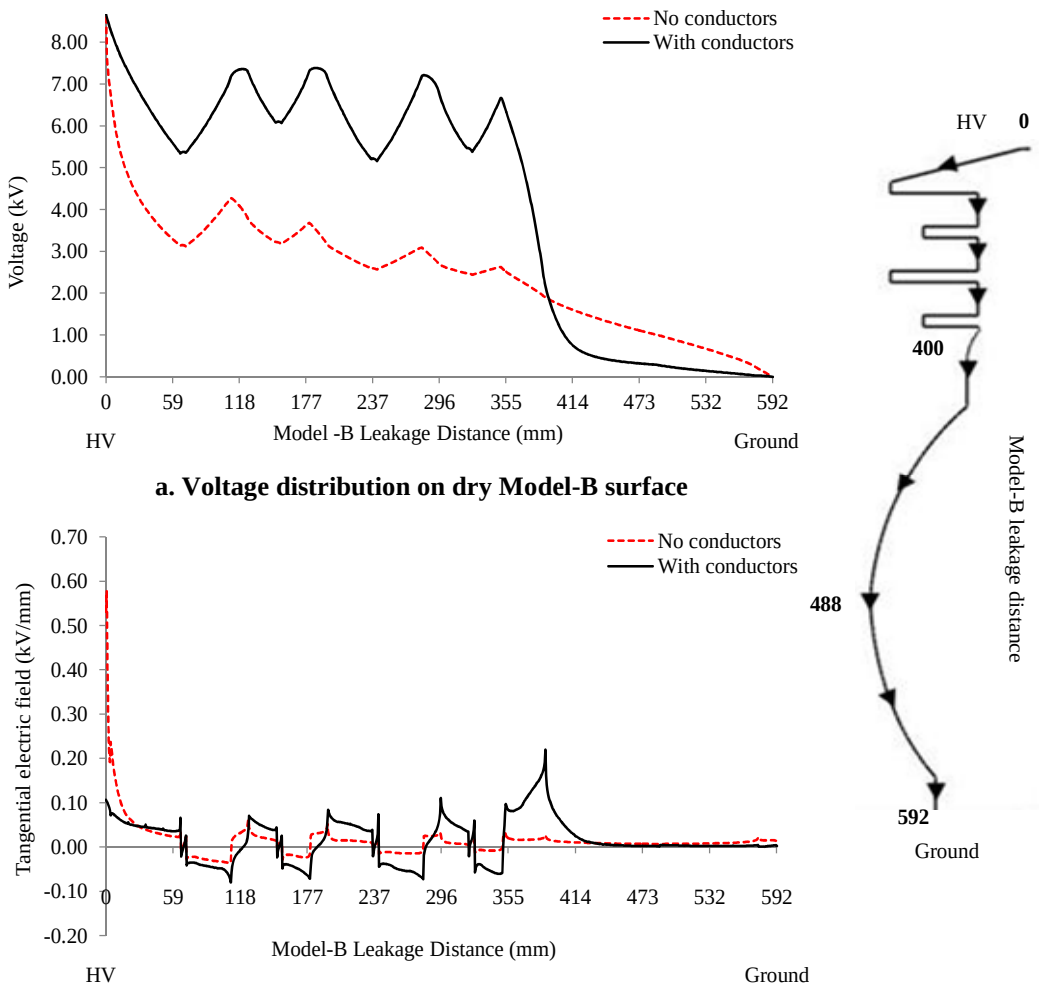

a. Voltage distribution on dry Model-B surface

b. Electric field distribution on dry Model-B surface

Figure 11. Voltage and electric field distribution on dry Model-B

Similar to the results for Model-A, Figure 11 shows the potential and electric field distribution along Model-B dry leakage length. For the case with conductors, consecutive big and small V-shapes form the voltage distribution plot for Model-B is due to voltage calculations made along the leakage length, similar to Model-A. However, due to the presence of four sheds and not more, there is a sudden dip of voltage after the sheds end at about 400 *mm*, causing an electric

field spike in that area, as observed from the electric field distribution plot from Figure 11. However, in the presence of internal conductors, the electric field calculations plotted do not show very high electric fields at any point along the Model-B leakage distance. The maximum electric field observed is about 0.2 *kV/mm* at a distance of about 400 *mm*. This value would perhaps have been lower and closer to ground if a fifth shed was included.

For the case with no conductors, from Figure 10 voltage distribution plot, it can be observed that the voltage drops largely when moving away from the HV end, causing a relatively high electric field stress of about 0.6 *kV/mm* at primary terminal-insulation system junction called the triple-point.

From the results obtained in Case 1, it can be concluded that internal conductors in dry and clean CTs distribute the electric fields stress along the entire surface as opposed to having high stress close to the HV end. Insulation system in dry-type CTs is expected to perform better in dry conditions than those in other electrical equipment which have no internal conductors. It can also be inferred that the number of sheds introduced to attain a high leakage length influences the voltage drop and position of electric field spikes on CT surfaces. For Model-A, five sheds results in high potentials close to ground and no electric fields spikes. For Model-B, four sheds results in low potential close to ground and a sharp electric field spike close to ground.

5.3. Case 2: Wet surface

In this section, potential and electric fields stress experienced on the insulation surface under wet conditions is reported. It documents results obtained when continuous and partial film of water forms on CT surfaces.

Continuous wetting

Figure 12 and Figure 13 show the voltage and electric field calculations along leakage distances of Model-A and Model-B CT with continuous film of water whose conductivity changes from 1 $\mu S/cm$ to 200 $\mu S/cm$. Results simulating CTs under conditions where the rate of wetting is higher than the rate of evaporation is reported.

From the voltage distribution plots in Figure 11 and Figure 12, it is noticed that the plots are not very different from their respective dry case plots. The difference is observed only in the depth of the V-shaped curves. Introducing a continuous film of water reduces the voltage drop as a continuous conducting path is available in the form of water films. The V-shaped curves observed in the dry case study are U-shaped when surface water is introduced. For example, considering Model-A with conductors, from Figure 10, drop in voltage from 8.66 kV to about 5 kV from 0 mm to 63 mm is observed when the surface is dry; and from Figure 12, the corresponding drop in voltage from 8.66 kV to 6 kV is observed for the 1 $\mu S/cm$ conductivity case and drop in voltage from 8.66 kV to 7 kV is observed for the 200 $\mu S/cm$ conductivity of wet case.

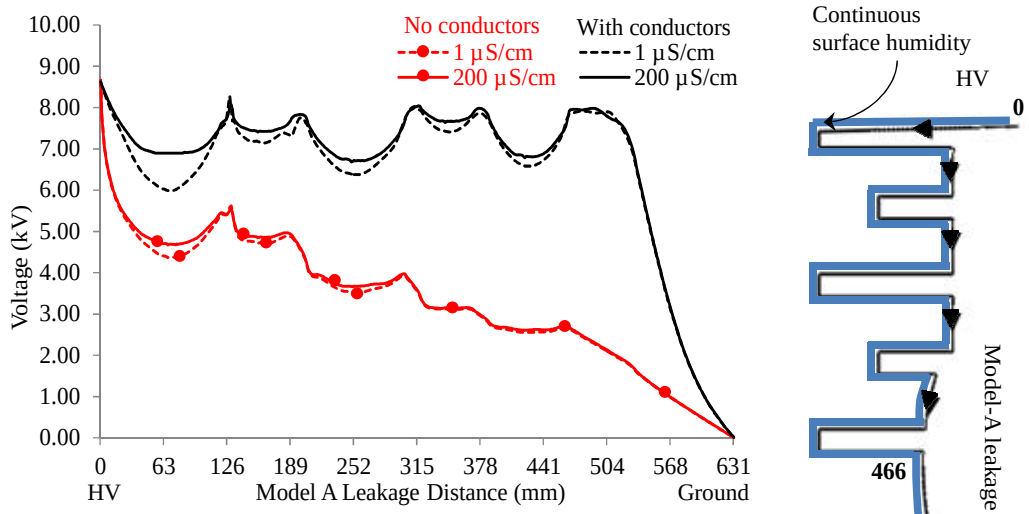

a. Voltage distribution on continuously wet Model-A surface

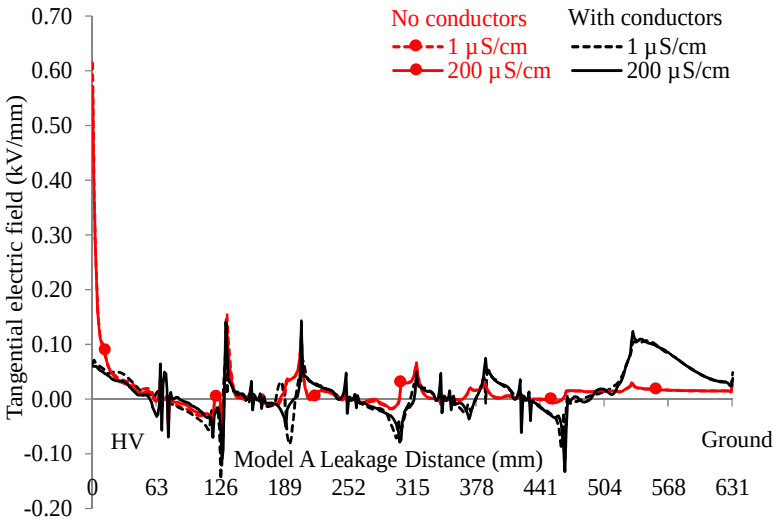

b. Electric field distribution on continuously wet Model-A surface

Figure 12. Voltage and electric field distribution with continuous wetting on Model-A

As the conductivity of water film increases, corresponding increase in current flow occurs. This results in lower voltage drops along the sheds, as observed

from voltage plots in Figure 12 and Figure 13. With regard to electric field plots, noticeable difference is only observed when comparing results with conductions and with no conductors. Similar to dry case, dry-type CTs have better outdoor performance than electrical equipment without any internal conducting parts.

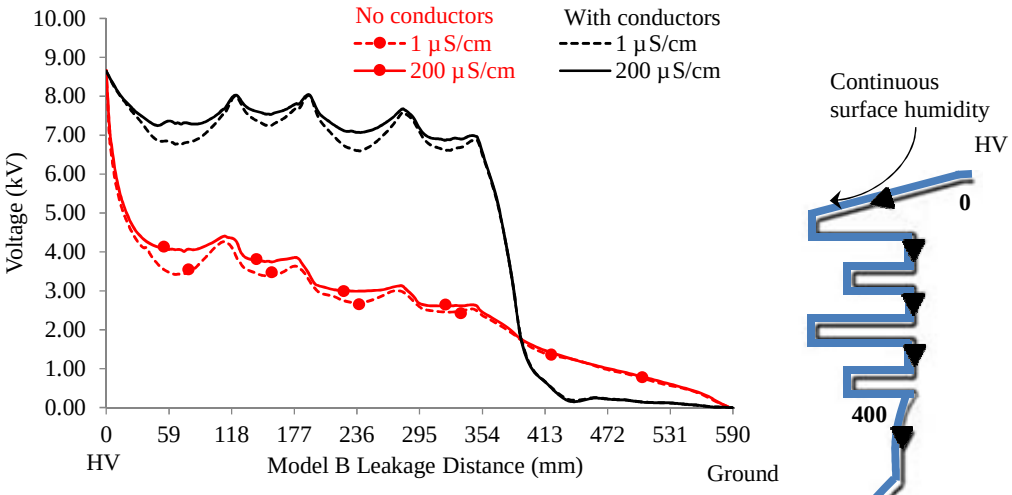

a. Voltage distribution on continuously wet Model-B surface

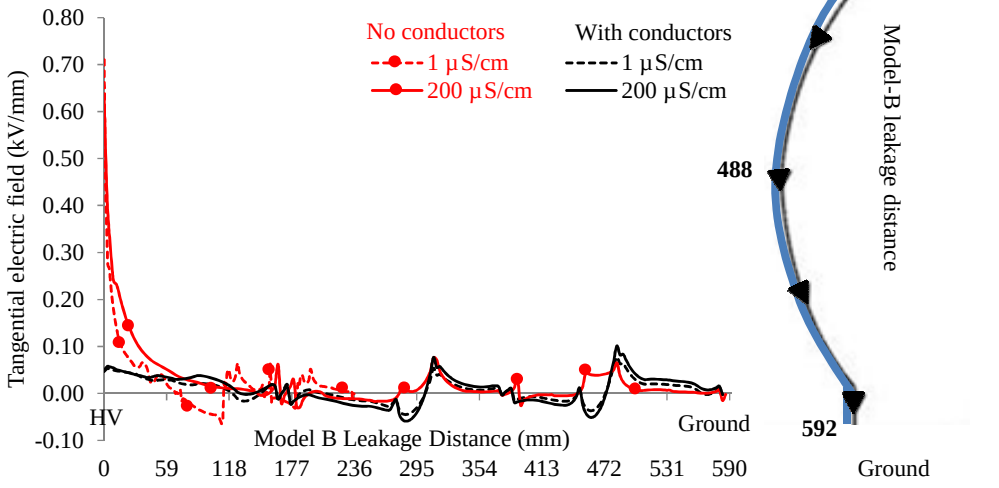

b. Electric field distribution on continuously wet Model-B surface

Figure 13. Voltage and electric field distribution with continuous wetting on Model-B

Partial wetting

Figure 14 and Figure 15 show the voltage and electric field calculations along leakage distances of Model-A and Model-B CT with broken or partial films of humidity whose conductivity changes from 1 $\mu S/cm$ to 200 $\mu S/cm$.

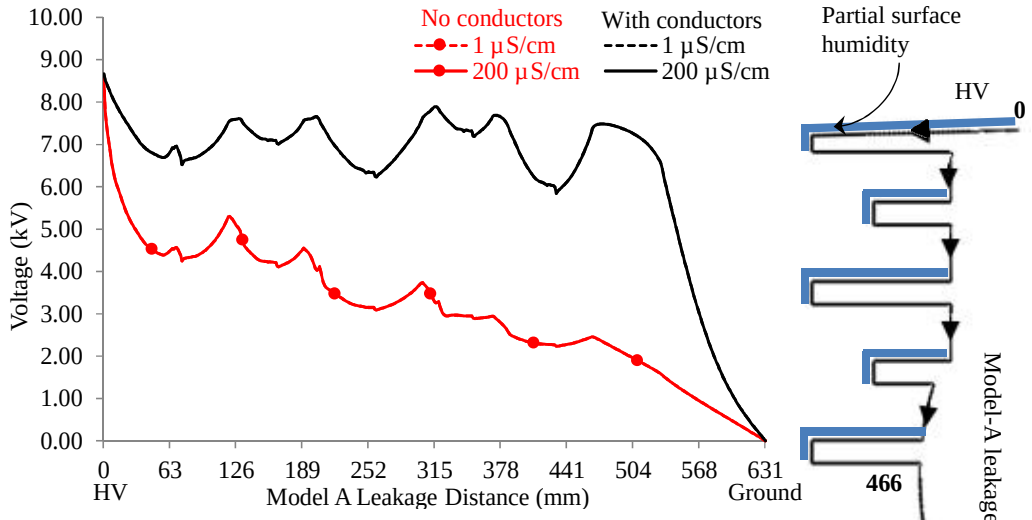

a. Voltage distribution on partially wet Model-A surface

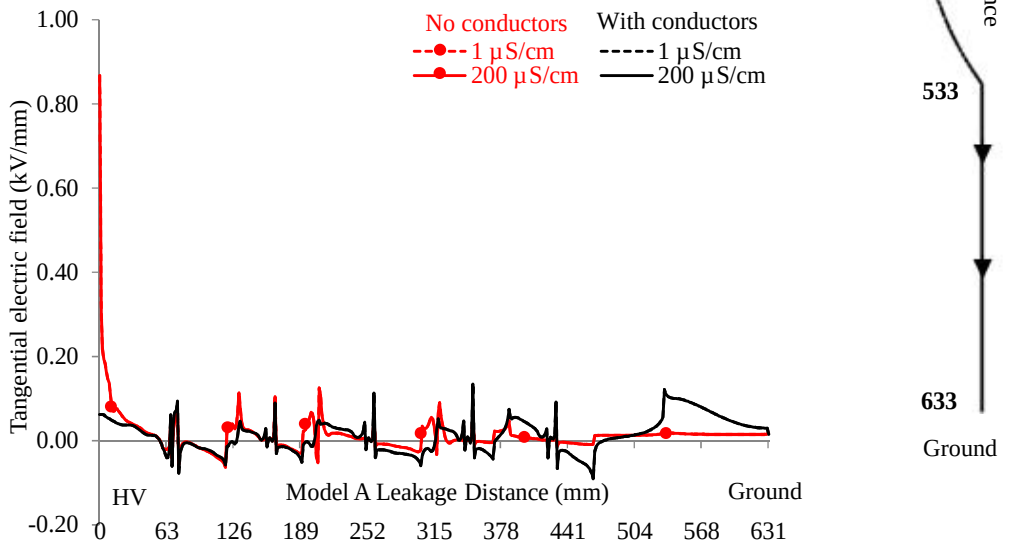

b. Electric field distribution on partially wet Model-A surface

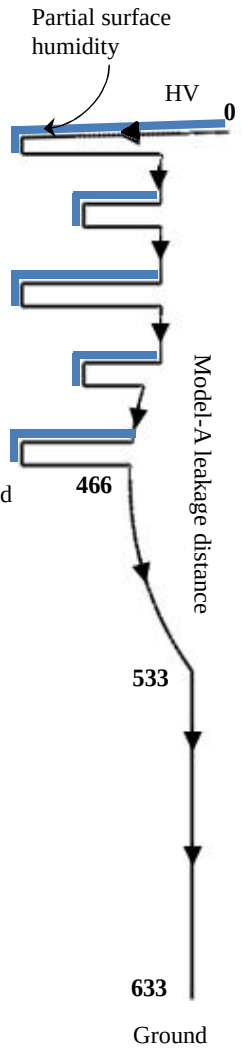

Figure 14. Voltage and electric field distribution with partial wetting on Model-A

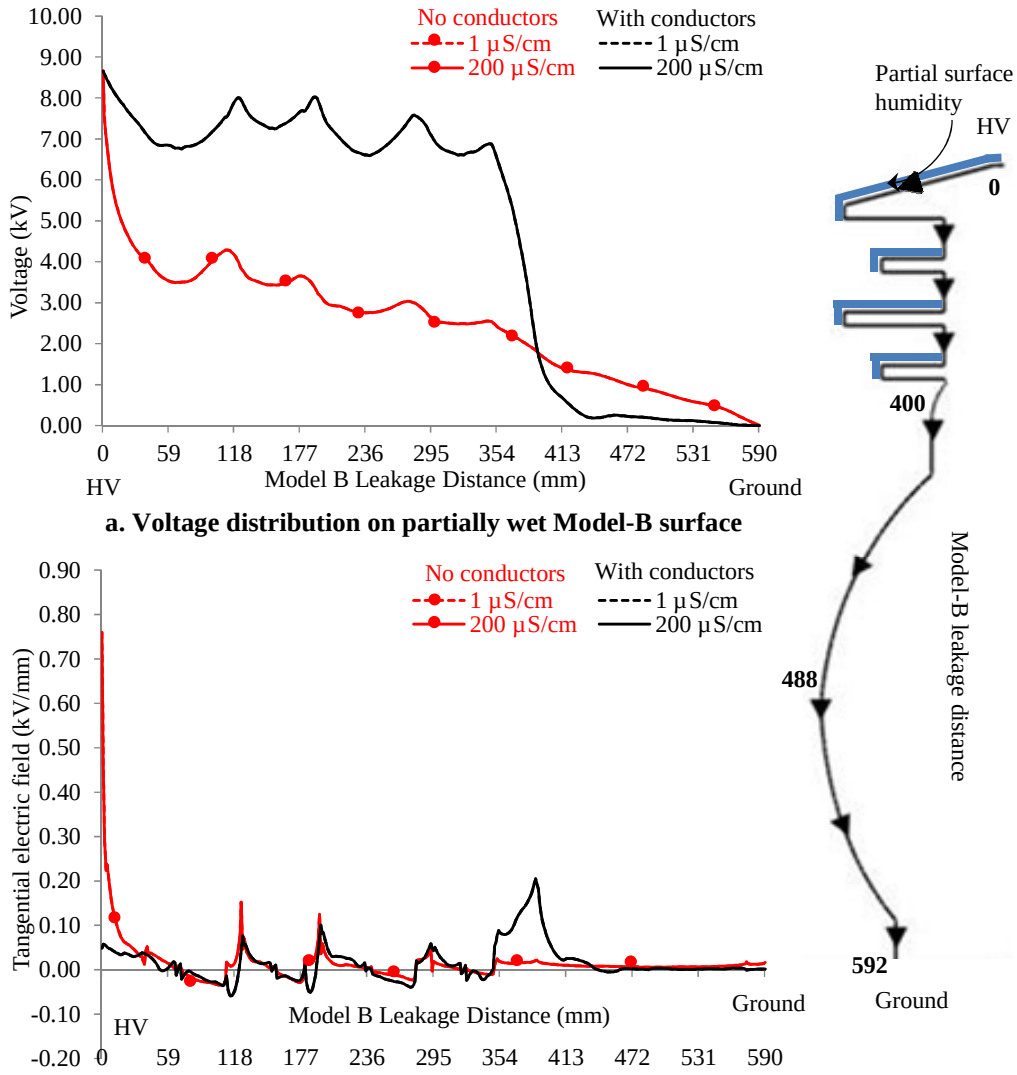

a. Voltage distribution on partially wet Model-B surface

b. Electric field distribution on partially wet Model-B surface

Figure 15. Voltage and electric field distribution with partial wetting on Model-B

From the plots shown in Figure 14 and Figure 15, it is evident that the change in conductivity of the water films does not have any affect. This can be attributed to the fact that, if a continuous film of humidity is not available, leakage currents on the surface will not flow. With no current flow the amount of conductivity offered by the humidity films does not affect the voltage or electric field distribution. The plots for different conductivity levels overlap each other as seen in Figure 14 and Figure 15. When the insulations system's surface is hydrophobic, situation arises where the water on the surface does not mega together to form a continuous conducting film. Therefore, on hydrophobic surfaces, the severity of contamination does not affect the surface voltage or electric field distribution as there is very less or no leakage current flow.

With regard to the electric field distribution plots in Figure 14 and Figure 15, it can be observed that, similar to the dry case, electric field stress is distributed and low when conductors are present and high at the triple-point when conductors are removed. The different is that, electric field spicks are observed at the humidity-insulation-air intersections where the water film ends. These localized spikes in electric field, if high, can cause dry band arcing and damage the insulation system surface. It can be concluded that the presence of internal conductors in dry-type CTs reduce the high electric field stress at the HV end under partially humid conditions. For the 15 *kV* line to line CTs considered in this thesis, the localized electric field spikes are under 0.2 *kV/mm* which is low and would not cause surface arcing

5.4. Case 3: Internal voids

Figure 16 and Figure 17 show the electric field calculations along voids place in the insulation structure of Model-A and Model-B CT, respectively. The calculations were made 20 mm inwards from the outer surface of the insulating material.

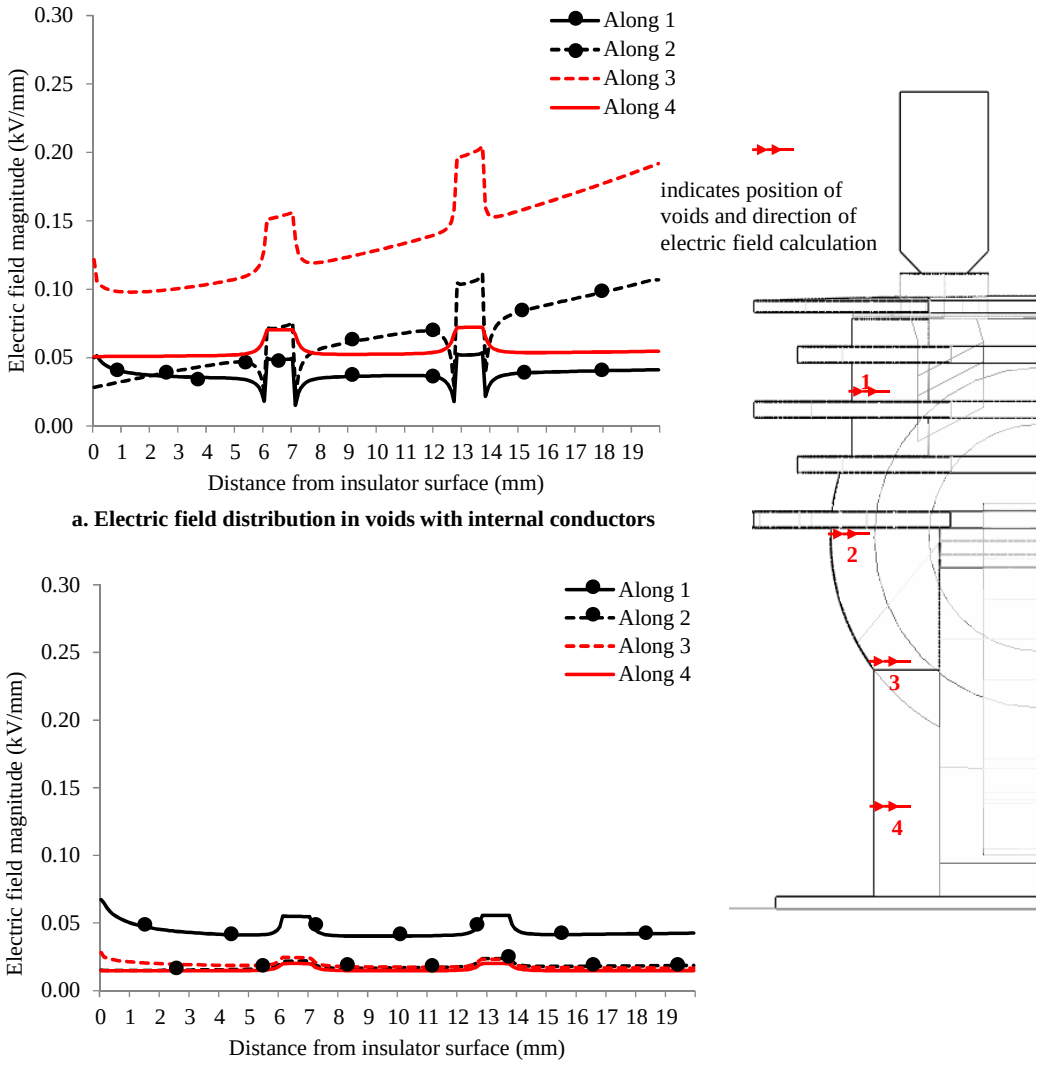

a. Electric field distribution in voids with internal conductors

b. Electric field distribution in voids without internal conductors

Figure 16. Electric field magnitude along 2 air voids located at different locations on Model-A

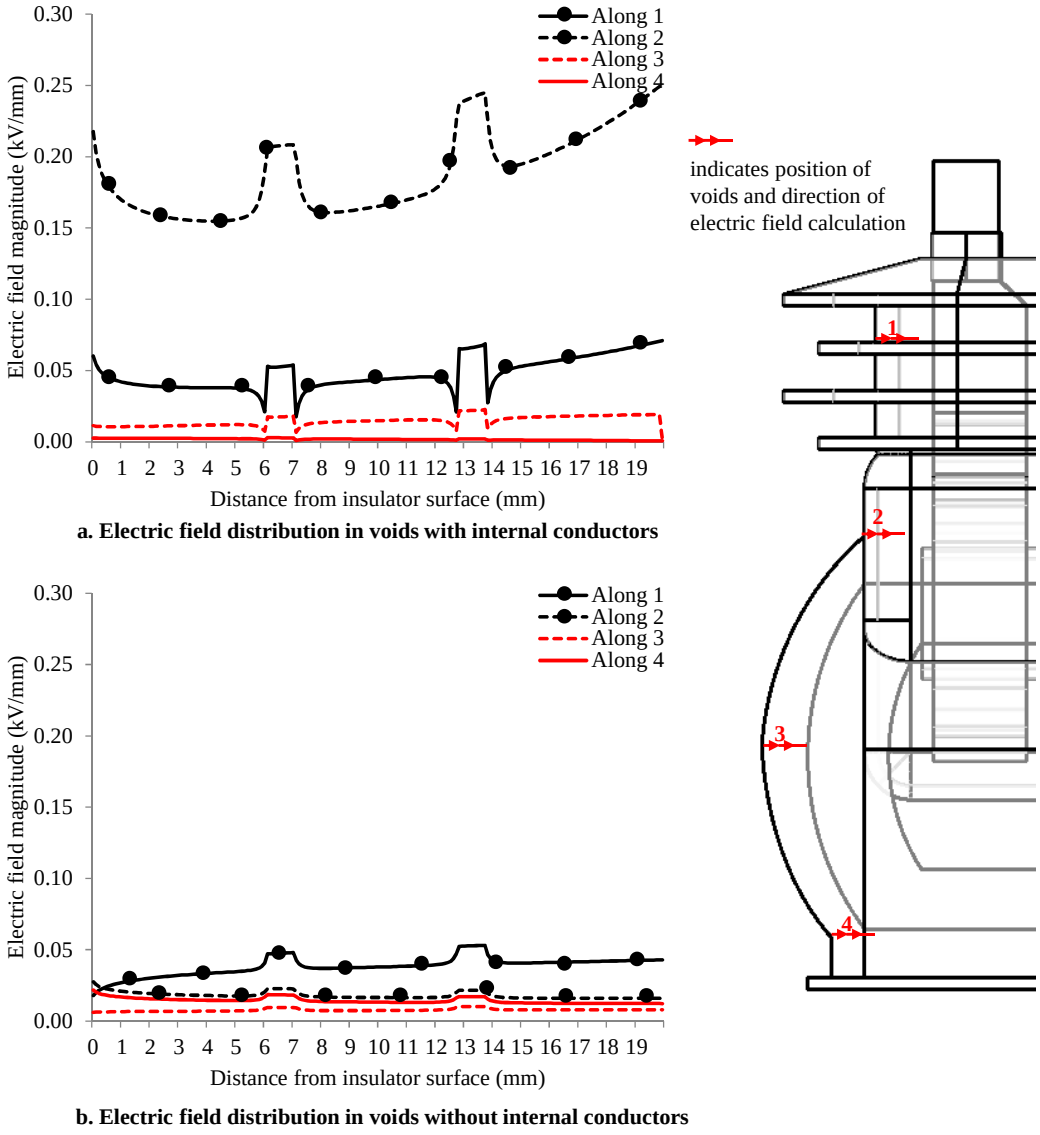

a. Electric field distribution in voids with internal conductors

b. Electric field distribution in voids without internal conductors

Figure 17. Electric field magnitude along 2 air voids located at different locations on Model-B

On comparing the electric field plots in Figure 16 and Figure 17 individually, it can be observed that when internal conductors are in place, the presence of voids result in high electric field stress across the voids. Also, the voids closer to the outer surface of the insulation system experience lesser electric field stress than those further inside.

Observing the electric field stress in voids at various locations of the CTs in Figure 16 and Figure 17, it can be seen that voids close to the mid-section of the CTs are experience the maximum electric field stress For Model-A the voids along calculation line 3 experience maximum electric field stress, and for Model-B the voids along calculation line 2 experience maximum electric field stress. On analyzing these calculations paths (along 3 for Model-A and along 2 for Model-B), it can be concluded that voids are most harmful at locations where the primary winding and the magnetizing core are coupled. It is important to avoid internal voids in dry-type CTs as the presence of internal conductors result in higher electric field stress when compared to electrical equipment with no internal conductors.

Chapter 6. CONCLUSION AND FUTURE WORK

6.1. Conclusions

This research was aimed at qualitatively analyze the effect of internal conductors on the performance and life expectancy of the insulation system used in dry-type medium voltage CTs. The boundary element method was used to simulate and investigate the effect of humidity and internal voids in CTs. The following conclusions can be drawn from the research documented in this thesis.

i. Computer analysis technique based on boundary element method is a powerful analysis tool for modeling and simulating different conditions on electrical equipment with complex geometries like CTs.

ii. Presence of internal conductors in CTs distribute the electric field stress along the entire leakage length, and hence result in better outdoor performance of CTs when compared to electrical equipment with no internal conductors.

iii. Presence of internal conductors makes the voltage distribution more uniform along the sheds.

iv. Number of sheds used to achieve a high leakage length influences the potential and electric field near the grounded base plate. High number of sheds results in high potential closer to ground, and low number of sheds results in an unwanted electric field spike.

v. Severity of contamination, i.e. the conductivity of films of water comes into the picture only when the insulation system surface is highly hydrophilic. Hydrophobic insulation surface causes contamination to not merge together to form a continuous conducting film from HV end to ground.

vi. Presence of internal voids is more harmful in dry-type CTs than in electrical equipment without internal conductors. Manufacturers need to be extra careful while binding insulation systems for dry-type CTs.

6.2. Future work

This research was focused on the quantitative analyses of the effect of internal conductors on voltage and electric filed distribution in dry-type CTs. As part of future work more CT models could be developed to build an analytical model that predicts the flashover voltage. Knowing the flashover mechanism in electrical equipment with no internal conductors, like outdoor insulators, formulas or algorithm could be developed to predict the flashover voltage in electrical equipment with internal conductors like bushings and transformers.

This research could be extended to accommodate insulation systems in medium voltage potential transformers (PTs), which have not been researched as part of this thesis. Using deterministic computer simulation results, like those in this research, Gaussian process models could be developed.

REFERENCES

[1] M. Yazdani-Asrami, M. Mirzaie, A. A. S. Akmal, "Investigation on impact of current harmonic contents on the distribution transformer losses and remaining life," IEEE International Conference on Power and Energy (PECon), pp.689-694, December 1 2010.

[2] J. Wimmer, M. R. Tanner, T. Nunn, J. Kern, "Dry-type - vs. - liquid-immersed transformers: Specification installation and operational impact in a marine environment," 2011 Record of Conference Papers Industry Applications Society 58th Annual IEEE Petroleum and Chemical Industry Conference (PCIC), pp.1-8, September 2011.

[3] J. Mackevich, M. Shah, "Polymer outdoor insulating materials. Part I: Comparison of porcelain and polymer electrical insulation," IEEE Electrical Insulation Magazine, vol. 13, no. 3, pp. 5-12, June 1997.

[4] D. A. Greenwood, W. N. Cottingham, *Electricity and Magnetism*, Cambridge University Press, Cambridge, 1991.

[5] B. D. Jenkins, *Introduction to Instrument Transformers*, CRC Press, Ohio, 1967.

[6] V. Y. Ushakov, *Insulation of High-Voltage Equipment*, Springer Press, New York, 2004.

[7] A. de la O, R. S. Gorur, "Flashover of contaminated nonceramic outdoor insulators in a wet atmosphere," IEEE Transactions on Dielectrics and Electrical Insulation, vol. 5, no. 6, pp. 814-823, December 1998.

[8] V. M. Moreno, R. S. Gorur, "Effect of long-term corona on non-ceramic outdoor insulator housing materials," IEEE Transactions on Dielectrics and Electrical Insulation, vol. 8, no. 1, pp. 117-128, March 2001.

[9] T. G. Engel, M. Kristiansen, "Mechanisms and predictors of insulator degradation and erosion produced by pulsed high-current surface discharges," IEEE Transactions on Plasma Science, vol. 37, no. 9, pp. 1863-1870, September 2009.

[10] K. Adamiak, J. M. Floryan, "Dynamics of water droplet distortion and breakup in a uniform electric field," IEEE Transactions on Industry Applications, vol. 47, no. 6, pp. 2374-2383, December 2011.

[11] A. Ahmed, H. Singer, P. K. Mukherjee, "A numerical model using surface charges for the calculation of electric fields and leakage currents on polluted insulator surfaces," Conference on Electrical Insulation and Dielectric Phenomena, vol. 1, pp. 25-28, October 1998.

[12] J. P. Holtzhausen, W. L. Vosloo, "The pollution flashover of ac energized post type insulators," IEEE Transactions on Dielectrics and Electrical Insulation, vol. 8, no. 2, pp. 191-194, April 2001.

[13] B. Sarang, V. Lakdawala, P. Basappa, "Electric field calculations on a high voltage insulator under wet conditions," IEEE Electrical Insulation Conference, Virginia, May 2009.

[14] J. S. Forrest, P. J. Lambeth, D. F. Oakeshott, "Research on the performance of high-voltage insulators in polluted atmospheres," Proceedings of the IEE - Part A: Power Engineering, vol. 107, no. 32, pp. 172-187, April 1960.

[15] T. Doshi, R. S. Gorur, J. Hunt, "Electric field computation of composite line insulators up to 1200 kV AC," IEEE Transactions on Dielectrics and Electrical Insulation, vol. 18, no. 3, pp. 861-867, June 2011.

[16] S. Monga, R. S. Gorur, P. Hansen, W. Massey, "Design optimization of high voltage bushing using electric field computations," IEEE Transactions on Dielectrics and Electrical Insulation, vol. 13, no. 6, pp. 1217-1224, December 2006.

[17] E. Kufel, W. S. Zaengel, *High Voltage Engineering Fundamentals*, Pergamon Press, 1988.

[18] W. W. Hansen, O. C. Lundstrom, "Experimental determination of impedance functions by the use of an electrolytic tank," Proceedings of the IRE , vol. 33, no. 8, pp. 528- 534, August 1945.

[19] S. Sima, F. P. Espino-Cortes, E. A. Cherney, S. H. Jayaram, "Optimization of corona ring design for long-rod insulators using FEM based computational analysis," Conference Record of the 2004 IEEE International Symposium on Electrical Insulation, pp. 480- 483, September 2004.

[20] P. B. Zhou, *Numerical Analysis of Electromagnetic Fields*, Springer-Verlag, Berlin, 1993.

[21] H. Singer, H. Steinbigler, P. Weiss, “A charge simulation method for the calculation of high voltage fields”, IEEE Transactions on Power Apparatus and Systems, vol. 93, pp. 1660-1668, 1974.

[22] S. Kaana-Nkusi, P. H. Alexander, R. Hackam, "Potential and electric field distributions at a high voltage insulator shed," IEEE Transactions on Electrical Insulation, vol. 23, no. 2, pp. 307-318, April 1988.

[23] M. M. A. Salama, A. Nosseir, R. Hackam, A. Soliman, T. El-Shiekh, "Methods of calculations of field stresses in a three-core power cable," IEEE Transactions on Power Apparatus and Systems, vol. 103, no. 12, pp. 3434-3441, December 1984.

[24] N. H. Malik, A. Al-Arainy, “Electric stress distribution in three core delted power cables,” IEEE Transactions on Power Delivery, vol. 2, no. 3, pp. 589-595, 1987.

[25] V. T. Kontargyri, I. F. Gonos, I. A. Stathopoulos, A. M. Michealides, "Simulation of the electric field on high voltage insulators using the finite element method," 2006 12th Biennial IEEE Conference on Electromagnetic Field Computation, pp. 373, 2006.

[26] Introduction to Boundary Element Method, available at: http://www.boundary-element-method.com, visited: May 2012.

[27] S. S. Bamji, A. T. Bulinski, K. M. Prasad, "Electric field calculations with the boundary element method," IEEE Transactions on Electrical Insulation, vol. 28, no. 3, pp. 420-424, June 1993.

[28] S. Monga, R. S. Gorur, W. Massey, "Electric field calculations by boundary element method for a 230 kV composite bushing," International Symposium 2005 IEEE Antennas and Propagation Society, vol. 3, pp. 338-341, July 2005.

[29] A. Wright, *Current Transformers – Their Transient and Steady State Performance*, Chapman and Hall Ltd., 1968.

[30] J. S. T. Looms, *Insulations for High Voltage*, Peter Peregrinus Ltd., London, 1988.

[31] Anonymous, *COULOMB® 9.0 Users and Technical Manual*, Integrated Engineering Software, 2011.

[32] S. Singha, M. J. Thomas, A. Kulkarni, "Complex permittivity characteristics of epoxy nanocomposites at low frequencies," IEEE Transactions on Dielectrics and Electrical Insulation, vol. 17, no. 4, pp. 1249-1258, August 2010.